Available online at www.HEFJournal.org

ISSN: 2785-2997

Journal of
Human, Earth, and Future

Vol. 6, No. 2, June, 2025

Enhancing Magnetotelluric Data Quality Using Deep Learning-Based Denoising Models: A Study of CNN and LSTM

Widya Utama [1*], Maman Hermana [2], Dwa D. Warnana [1], Wien Lestari [1], Muhammad N. A. Zakariah [2], Sherly A. Garini [1, 3], Rista F. Indriani [1, 4], Dhea P. Novian Putra [1], M Ulin Nuha Abduh [1], Alif N. F. Insani [1], Dandi Syahtia Pratama [1], Khairul Arifin Mohd Noh [2], Abdul Halim Abdul Latiff [2]

[1] *Department of Geophysical Engineering, Institut Teknologi Sepuluh Nopember, Surabaya, 60117, Indonesia.*

[2] *Department of Geosciences, Universiti Teknologi Petronas, Seri Iskandar, 32610, Malaysia.*

[3] *Department of Informatics, Institut Teknologi Sepuluh Nopember, Surabaya, 60117, Indonesia.*

[4] *Department of Geomatics Engineering, Institut Teknologi Sepuluh Nopember , Surabaya, 60117, Indonesia.*

Received 28 November 2024; Revised 26 April 2025; Accepted 05 May 2025; Published 01 June 2025

Abstract

Noise interference in Magnetotelluric (MT) signals significantly undermines the accuracy of subsurface resistivity analysis, leading to potential errors in geophysical interpretation and challenges in resource exploration. To address this critical issue, this study develops denoising models based on Convolutional Neural Networks (CNN) and Long Short-Term Memory (LSTM) to enhance the quality of MT signals while preserving their original structure. The proposed models utilize MT data, incorporating electric field (E) and magnetic field (H) components, to effectively reduce noise. Evaluation results demonstrate that CNN outperforms LSTM, increasing the Signal-to-Noise Ratio (SNR) by up to 58.8% (or 1.6 times) in the Hx channel. CNN also records lower Normalized Mean Square Error (NMSE) values across all channels, ranging from 0.006 to 0.033, while maintaining a high correlation coefficient of 0.999 in the Hz channel. Moreover, CNN is significantly faster, with processing times of 24.83 to 29.16 seconds—up to three times faster than LSTM, which requires 67.38 to 70.69 seconds. The superior performance of CNN in mitigating noise in MT data is attributed to its architecture, which focuses on local patterns. This makes it particularly effective for handling localized and sporadic noise, as observed in the Hx and Hy channels with recurring amplitude patterns. In contrast, LSTM is less effective for MT data with unstructured noise, such as in the Hz channel, due to its sequential approach, which is better suited for capturing long-term temporal relationships. This study aligns with the Sustainable Development Goals (SDGs), specifically SDG 9, which promotes innovative applications of deep learning technology, and SDG 7, which emphasizes improving the accuracy of renewable energy exploration. The findings provide a foundation for developing more adaptive and efficient denoising models, contributing to environmental sustainability and the advancement of clean energy exploration in the future.

Keywords: Convolutional Neural Network (CNN); Denoising, Noise; Long Short-Term Memory (LSTM); Magnetotelluric (MT).

1. Introduction

The Magnetotelluric (MT) method represents a widely utilized approach for geothermal resource analysis through the subsurface identification based on electrical resistivity as a physical properties model [1, 2]. This method involves

* Corresponding author: widya@geofisika.its.ac.id

http://dx.doi.org/10.28991/HEF-2025-06-02-010

the measurement of natural variances in electromagnetic wave phenomena, which are induced by solar activity, geomagnetic storms, and lightning [3]. The electromagnetic wave covers a wide-range of frequencies, from 0.0001 Hz to 10,000 Hz [4, 5]. MT method reliability depends on their natural signal sources, making it vulnerable to environmental noise interference [6]. Industrial development and urbanization have grown faster and contaminated MT signals with noise [7, 8]. Nowadays, MT surveys near mountainous areas also encountered challenges due to measurement points surrounded by the roads, residential areas, telecommunication cables, and power lines in a relatively short radius. Due to its spatial closeness with MT signal noise source, it will be difficult to achieve smooth resistivity curves, especially in the modeling of deeper resistivity structures. Without effective noise reduction, MT signals can be distorted, leading to the loss of important resistivity information [9, 10]. Therefore, denoising process is essential for enhancing MT data quality, minimizing distortions, ensuring data accuracy, and unbiased data interpretation [10, 11].

Several conventional methods have been developed to reduce noise in MT data (e.g., multivariate robust processing, cross power selection, singular value decomposition) [12–16]. These methods utilized remote reference and discrete wavelet transform that have been widely applied, but still have limitations in reducing specific electromagnetic noise (e.g., vehicle vibration, active electricity cable line) [15, 16]. A primary issue in these methods is the ineffectiveness in handling diverse noise characteristics and requiring manual intervention during its processing [17]. One of manual interventions in the conventional MT signal denoising involves manual adjustment to set the window function for different frequencies and parameters [18]. Another conventional approach based on the remote reference method, that is considered less effective depends on its high frequencies of reference data, where it is problem when noise is identified at low frequencies (lower than 1 Hz) [17, 19].

Usage of machine learning has emerged as a prominent approach in geophysical exploration in recent studies [20–24]. Machine learning algorithms are promising complex pattern recognition in geophysical data and producing precise results rather than conventional methods [25–28]. Machine learning algorithms like Support Vector Machines (SVM) and Decision Trees (DT) have been used to predict the subsurface permeability model based on its porosity and dynamic viscosity [25, 28]. As part of machine learning, Deep Learning (DL) represents deep-seeking data correlation analysis and developing for more complex applications in geophysical modelling. Convolutional Neural Networks (CNN) and Long Short-Term Memory (LSTM), both of which have proven highly effective in signal processing, are categorized as DL algorithms, whereas in MT signal denoising is preferred due to their adaptability to various noise types [26, 27].

The significant advantage of utilizing CNN in signal processing is its ability to extract local features from data [29, 30]. CNN algorithm utilizes convolutional layers that potentially detect local patterns in MT signals, which particularly contain important subsurface data in pattern recognition and signal classification [31–33]. Experimental results have shown the CNN algorithm was highly effective in identifying noise and reconstructing clean signals in MT data, achieving high Normalized Cross-Correlation (NCC), and low Normalized Root Mean Square (NRMS) error, which reflects its ability to preserve original features [34]. Furthermore, the modelling process using CNN algorithm is efficient, where requiring approximately 92 seconds only of training time for relatively large datasets [26]. On the other hand, LSTM also demonstrated strong performance in denoising time-series data with effectively removing noise while preserving essential features of the original data [31, 33]. Previous studies have shown LSTM's effectiveness in meteorological time-series forecasting, such as predicting daily average temperatures with relatively low Root Mean Squared Error (RMSE) [35]. LSTM has also been used for denoising electrocardiogram (ECG) signals affected by severe noise, including random and drifting noise [36]. These multi-purpose application of CNN and LSTM algorithms in the denoising signal patterns shows its ability to address general and specific noise data cleaning, especially in MT signal denoising process.

Most of the research in MT signal denoising utilizes one machine learning algorithm [26, 33, 36, 37]. There is limited research in the MT signal denoising that uses qualitative and quantitative comparison analysis to determine the better algorithm that used in the specific MT survey area [31, 33]. Several studies about MT signal denoising took place in the electromagnetic noisy area (e.g., city center, industrial area) [26, 27, 38]. There is still little research on MT signal denoising based on MT surveys in the mountainous area, whereas the residential area nowadays also spreading in those areas, which potentially affect MT signal measurement [9]. This research intentionally addresses those problems using MT signal measurement in the mountainous area, near residential and power cable lines, that potentially affect MT signal noise. Specifically, this research utilizes MT data collected from Kirishima volcano in Japan [39]. The dataset, identified as KHZ043, and has been applied in remote reference calibration as validated by Triahadini et al. (2023) [9]. This dataset provides a reliable reference for addressing electromagnetic noise challenges in mountainous environments, making it ideal for validating the proposed CNN and LSTM-based denoising approaches.

This research using both CNN and LSTM algorithms that offer advanced methodologies for denoising MT signal data. CNN offers effective time processing and accuracy in extracting local features, making it highly effective at identifying noise and reconstructing clean signals [26, 32, 34, 40, 41]. LSTM offers deep analysis at capturing temporal patterns, which has been proven in handling noise within time-series data [31, 35, 36, 42, 43]. This research

compares different methods to find the best algorithm among CNN and LSTM in terms of its utilization in MT signal data cleaning. This research supports Sustainable Development Goals (SDGs) by improving the quality of geophysical data, which focuses on innovation by advanced technology (SDGs no. 9) and affordable clean energy through efficient renewable energy monitoring and evaluation (SDGs no. 7). This research results have the outcome to accelerate the eco-friendly technologies invention, promote effectiveness in energy-saving, and to preserve environment for future generations.

The structure of this article is as follows: Section 2 outlines the research methodology, including details on the dataset and data preprocessing stages, such as noise identification, feature scaling, and synthetic noise generation for training data. It also covers model development using CNN and LSTM algorithms, as well as model evaluation. Section 3 presents the experiment results and discussion. Finally, Section 4 provides the conclusions, along with a concise summary of the key decisions made in the preceding sections.

2. Research Methodology

The objective of this study is to develop Magnetotelluric (MT) signal denoising models based on deep learning algorithms, CNN and LSTM, to automatically reduce noise while enhancing the quality of MT signals. The process begins with the collection of MT data, where noise-contaminated signals undergo preprocessing. This includes the identification of noise in real MT data and the construction of synthetic noise based on the identified criteria. Subsequently, the CNN and LSTM deep learning models are trained using prepared training data, focusing on their ability to recognize and denoise noise [18, 20, 22]. The models are then evaluated using performance metrics, including Signal-to-Noise Ratio (SNR), correlation coefficient, and Normalized Mean Square Error (NMSE), to assess their effectiveness in improving signal quality, as illustrated in Figure 1.

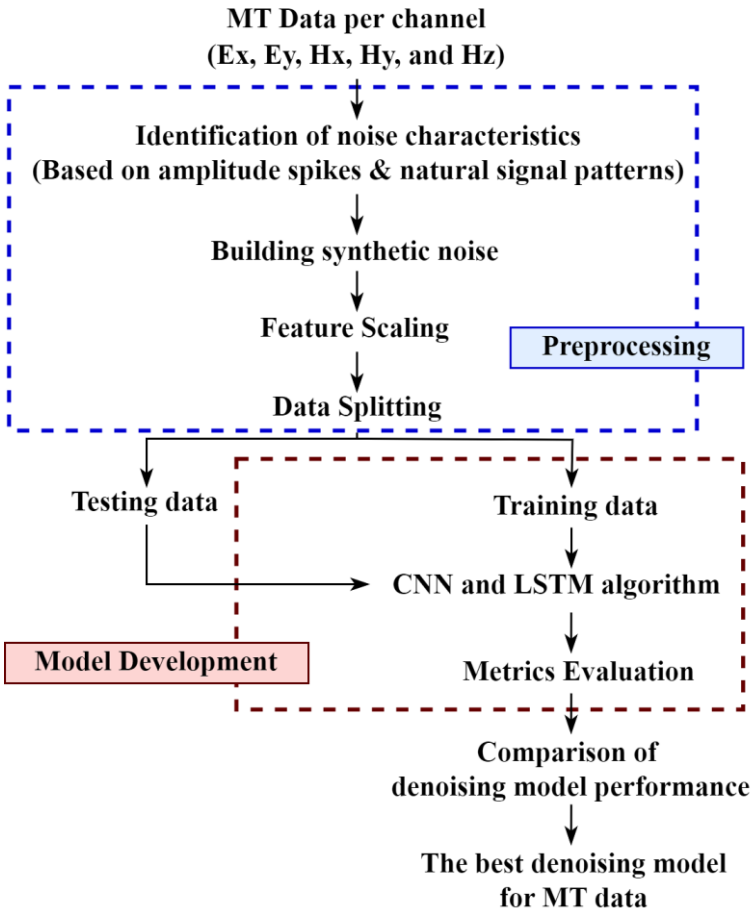

Figure 1. Research Workflow

2.1. The Dataset

The MT data used in this research project consist of field data collected from the Kirishima volcano in Japan, as illustrated in Figure 2. The dataset, identified by the code KHZ043, originates from the original work of Dr. Koki Aizawa at the Institute of Seismology and Volcanology, Kyushu University, as specifically detailed in Aizawa et al. (2014) [39]. This dataset has also been used in several previous studies for remote reference calibration, including the study by Triahadini et al. (2023) [9].

The dataset comprises 100,000 time-series MT data points, including five main signal components: two electric field components (Ex and Ey channels) and three magnetic field components (Hx, Hy, and Hz channels), as depicted in Figure 2. The y-axis in the graph represents the signal amplitude for each component of the electric field (Ex and Ey) and the magnetic field (Hx, Hy, and Hz), where variations in values indicate the magnitude and direction of field changes over time. The dataset is divided into 80% training data and 20% testing data [41, 44].

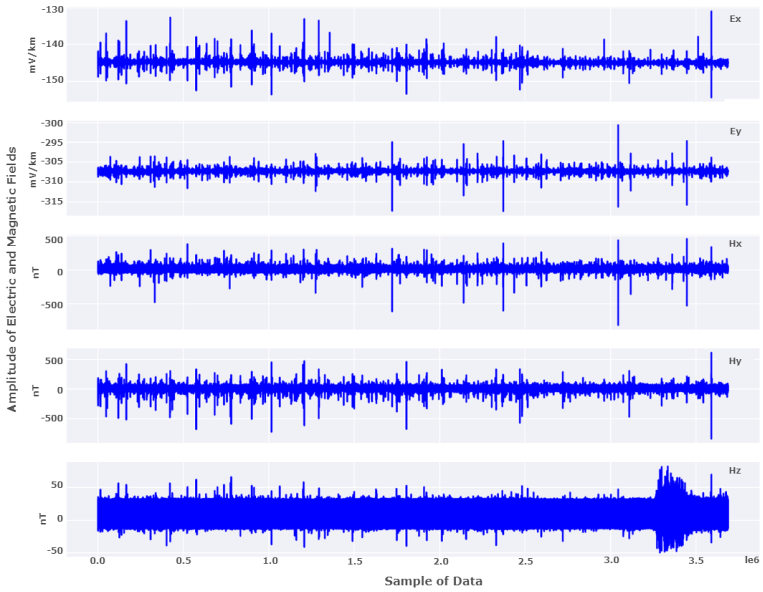

Figure 2. Visualization of MT Data Showing Variations in Electric Fields (Ex, Ey) and Magnetic Fields (Hx, Hy, Hz)

2.2. Preprocessing Data

At this stage, several essential steps are carried out to prepare the raw MT data prior to model development. The process begins with noise identification and feature scaling, followed by the generation of synthetic noise for training data. This is then followed by model development and performance evaluation of the deep learning models [31, 45].

2.2.1. Noise Identification

Noise identification in this study is based on the presence of amplitude spikes and unnatural signal patterns. A qualitative approach is employed by observing amplitude spikes and irregular signal patterns to determine the presence of noise in MT signals [4, 8, 18]. Noise in MT signals typically exhibits amplitude values that can reach up to ten times higher than normal signal amplitudes. Based on this, noise identification is also performed quantitatively by examining the amplitude magnitude. Figure 3 illustrates an example of noise segment identification in the electric field component (Ex channel) [18].

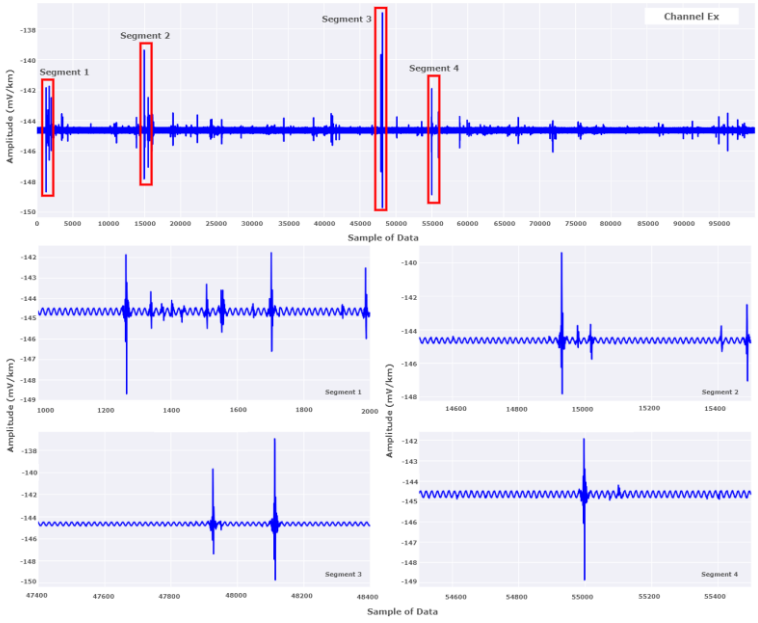

Figure 3. Identification of Noise Segments and Four Key Segments Characterized by Noise (Example from Ex Channel)

$$Average\ of\ maximum\ amplitude = \frac{1}{4}\sum_{i=1}^{4} M_i \quad (1)$$

Table 1. Maximum Amplitude in Each Noise Segment (Example: Ex Component)

Segment (M_i)	Maximum Amplitude
1	-141.76
2	-139.39
3	-136.95
4	-141.92

The maximum amplitude for each segment identified as noise is then calculated, as shown in Table 1. The noise in the MT data used in this study was introduced synthetically. The noise was designed based on the prior identification of amplitude spikes and irregular signal patterns in the original MT data. This process was carried out to simulate disturbances or anomalies in MT signals. Synthetic noise is considered representative of real-world noise because it was designed to mimic the characteristics of actual noise, including high amplitudes that can reach up to ten times greater than normal signal levels [18]. Subsequently, the average value of the maximum amplitude is calculated using Equation 1. Noise identification is conducted for each component, specifically the two electric field components (Ex and Ey channels) and the three magnetic field components (Hx, Hy, and Hz channels).

2.2.2. Feature Scaling

Feature scaling is a crucial step to ensure that all features are on the same scale, allowing algorithms to learn more effectively and stably. One commonly used method is the min-max scaler, which transforms feature values into a specified range, typically between 0 and 1, without altering the relative distribution between values [25, 26]. Equation 2 is the formula used to normalize the average maximum amplitude values in this study [23].

$$Average\ of\ maximum\ amplitude\ normalized = \frac{\frac{1}{4}\sum_{i=1}^{4} M_i - y_{min}}{y_{max} - y_{min}} \quad (2)$$

where M_i represents the maximum amplitude value of each segment, y_{min} is the minimum value of the dataset, and y_{max} is the maximum value of the dataset. The normalized values are then used as input for spike amplitude in the process of generating synthetic noise data [27].

2.2.3. Generating Synthetic Noise for Training Data

The next step involves generating synthetic noise to enrich the variety of noise in the training data. This synthetic noise is constructed based on the identification results from the previous step, ensuring that the synthetic noise is proportional and realistic in accordance with actual MT data. The addition of synthetic noise is performed using the Python function "add_spike_noise", where several random indices in the data are selected to introduce "spikes" with amplitude values (spike_amplitude) derived from the earlier identification process. The number of spikes added is controlled by the parameter num_spikes, while the direction of the spikes (positive or negative) is randomly chosen using np.random.choice ([-1, 1]), ensuring variation in each noise spike. This function also preserves the original data by creating a copy before modifying the selected indices. A visualization of the synthetic noise generation results for the Ex component can be seen in Figure 4 [28].

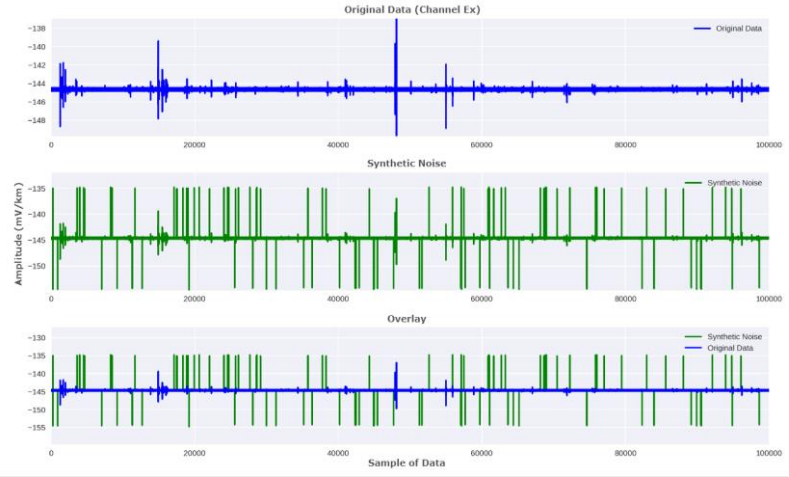

Figure 4. Process of Generating and Adding Synthetic Noise to the Ex-Channel

The visualization in Figure 4 provides an understanding of how synthetic noise is added, using the Ex channel as an example. The first graph in Figure 4 displays the original signal data, with some residual noise assumed to remain. This original data serves as a baseline for comparison with the results after the addition of the constructed synthetic noise. In the second graph, the successfully generated synthetic noise is marked by spikes in several segments of the signal. This noise is randomly added to simulate disturbances or anomalies in the MT signal. The third graph, an overlay of the original data and the synthetic noise, offers a direct comparison between the two. The blue line represents the original data, while the green line indicates the added noise. The steps applied to the Ex channel are also implemented for the other five channels (Ey, Hx, Hy, and Hz). The final stage of preprocessing involves data splitting, where the dataset is divided into training and testing data. These preprocessing steps ensure that the developed model is built using high-quality data, enabling it to handle diverse noise patterns effectively during training and testing [28]. This approach was applied to all MT data components (Ex, Ey, Hx, Hy, and Hz) to ensure realistic and diverse representations during model training.

2.3. Model Development

The deep learning approach used in this research offers a superior solution with outstanding capabilities in handling complex and diverse data patterns. The two main algorithms used are CNN, which excels at extracting local features from data, and LSTM, which is adept at understanding complicated temporal patterns and capturing long-term relationships in sequential data [29].

2.3.1. CNN Algorithm

In the process of MT signal denoising, the development of an effective model is essential to handle the various types of noise that appear in the data. One method that is often used due to its superior ability to process signals is the Convolutional Neural Network (CNN). CNNs are well suited for this task as they can extract local features from signal data, recognize important patterns, and automatically identify and reduce noise with higher accuracy than conventional methods [15]. The CNN architecture itself is inspired by biological processes in the human visual cortex, where neurons respond to local stimuli, enabling efficient feature extraction [30, 31]. In this study, the process of denoising MT signals with CNN starts from the input layer, which receives MT time-series signal data that still contains noise. Convolutional layers then apply kernels to extract important features and ignore noise, resulting in feature maps that store relevant information from the signal. After that, the fully connected layers process all the features to separate the noise from the original signal. At the output layer, a noise-cleaned MT signal is produced and ready for further analysis. CNN utilizes convolution to effectively separate noise from the original signal. The CNN architecture can be seen in Figure 5 [32, 33].

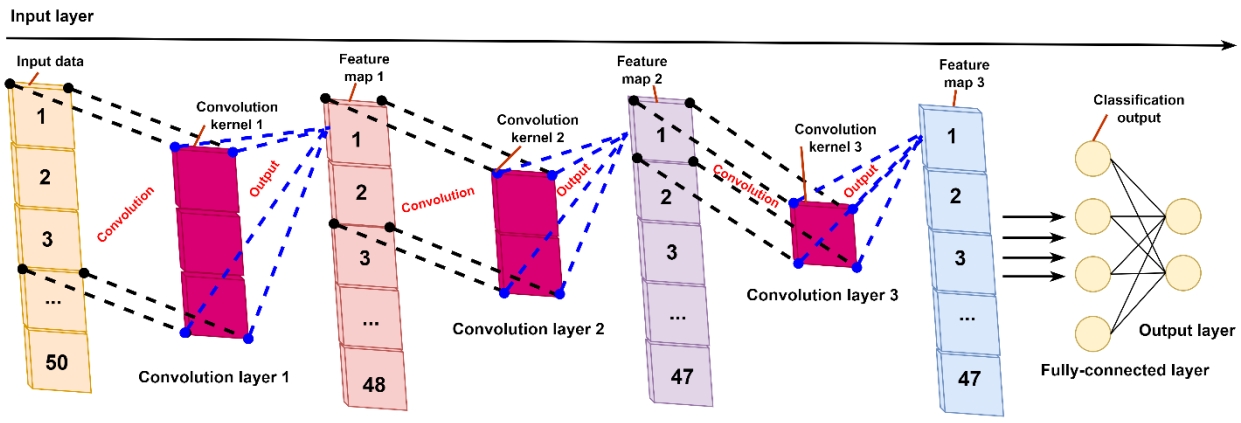

Figure 5. CNN Architecture [46]

The parameters of the CNN algorithm model used for the training process in this study are shown in Table 2, with default values applied. The structure and layers of the CNN model can be seen in Table 3. These parameters play a critical role in the training process to generate clean signal predictions for the denoising process. The Adam Optimizer parameter is used to iteratively update the network weights based on the training data. The batch size determines the number of samples processed before updating the model's internal parameters. Batch size is a type of hyperparameter in deep learning algorithms, where smaller batch sizes provide more detailed information from the training data. However, excessively small batch sizes may lead to overfitting, where the model performs exceptionally well during training but struggles to predict accurately on testing data. The epoch specifies the number of times the deep learning algorithm processes the entire dataset, both forward and backward. The activation layer/function, such as ReLU, determines whether neurons should be activated based on the weights and inputs provided. This enhances the efficiency of the denoising process [34, 35].

Table 2. Training Parameters of the CNN Model for the Denoising Process

Parameters	Description
Batch size	64
Epoch	100
Activation layer	ReLU
Optimizer	Adam
Learning rate	0.001

Table 3. Layer Structure and Function in CNN Model for Denoising

No	Layer/Block	Parameters	Purpose
1	Bidirectional LSTM Layer	- Units: 64 - Bidirectional: Yes - Return Sequences: True	Capturing temporal relationships in the data from both forward and backward directions to enhance model accuracy [47].
2	Dropout Layer	- Rate: 0.2	Reducing the risk of overfitting by randomly dropping some units during training [48].
3	LSTM Layer	- Units: 32 - Return Sequences: True	Capturing additional temporal relationships from previously processed sequential data to model more complex patterns [49].
4	Dropout Layer	- Rate: 0.1	Reducing the risk of overfitting in subsequent layers after the second LSTM layer [48].
5	Time Distributed Dense Layer	- Units: 32 - Activation: ReLU	Applying a Dense Layer to each timestep independently to effectively combine features [50].
6	Output Time Distributed Dense	- Units: 1	Generating final predictions for each timestep in the input sequence based on the learning outcomes of the entire network [50].

2.3.2. LSTM Algorithm

LSTM identifies temporally distributed noise patterns through its specialized memory structure, which is designed to store and manage essential information over extended periods. The architecture of LSTM, as illustrated in Figure 6, includes key components such as memory cells and three primary gates: the input gate, the forget gate, and the output gate. These gates work together to selectively regulate which information should be retained, discarded, or used. The input gate controls the information entering the memory, the forget gate removes irrelevant information, and the output gate determines which information will be generated as output at each time step [40, 41]. This structure enables LSTM to effectively retain critical signals while eliminating irrelevant noise from sequential data [42]. In the application of MT signal denoising, LSTM is expected to perform effectively due to its ability to recognize patterns in time-ordered data. The model can identify essential patterns within sequential data while filtering out noise, producing a cleaner signal without compromising vital information. The recursive nature of LSTM allows the model to "remember" previous information while processing data, enabling it to account for temporal relationships within the dataset. The training parameters for the LSTM model used in the denoising process are detailed in Table 2, while the structure and layers of the LSTM model are presented in Table 3 [43].

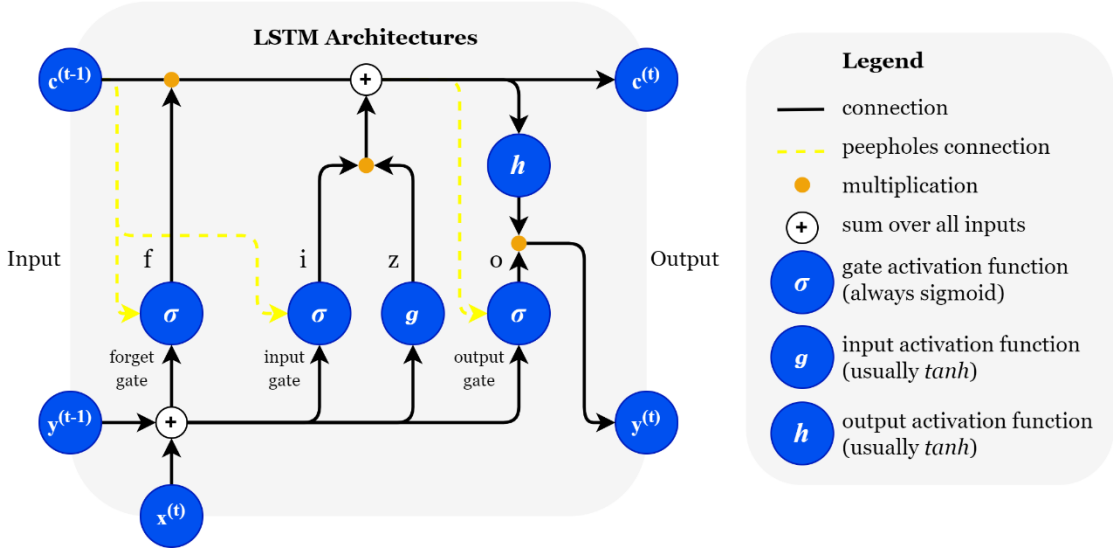

Figure 6. LSTM Architecture [49]

In this study, another notable difference is the use of model regularization. LSTM employs a dropout layer, whereas CNN does not. This distinction reflects the architectural characteristics of each model, influencing how data is processed and the potential risk of overfitting. In LSTM, dropout is necessary due to its sequence-based nature and its ability to retain information in memory cells for extended periods. This increases the risk of the model memorizing patterns excessively, which can lead to overfitting [51]. To mitigate this issue, dropout is applied as a regularization technique by randomly deactivating a subset of neurons during training. This prevents the model from becoming overly reliant on specific neurons and enhances its ability to generalize across different data [33].

In contrast, CNN does not require a dropout layer, as its architecture is inherently more resistant to overfitting. Parameter sharing in CNN's convolutional layers significantly reduces the number of parameters that need to be learned, thereby preventing excessive model complexity [33]. Additionally, the use of pooling layers helps reduce feature dimensionality, further minimizing the risk of overfitting. With this mechanism, CNN can achieve good generalization without the need for additional regularization techniques such as dropout. The consistent use of hyperparameters, including the Adam optimizer, learning rate, and batch size, in this study (Tables 2 and 3) ensures a fair performance comparison between the two models, isolating the differences in results solely to their architectural characteristics [52].

2.4. Model Evaluation

Once the CNN and LSTM models have been successfully developed for MT signal denoising, the next step is to evaluate the models to assess how effectively they remove noise from the signals. This evaluation is crucial to ensure that the models can accurately and consistently separate noise and remain reliable when applied to new data. Several evaluation metrics are used during the performance evaluation stage of this research, including signal-to-noise ratio (SNR), normalized mean square error (NMSE), and correlation coefficient. These metrics provide a comprehensive measure of the accuracy of the denoising results achieved by the deep learning models [53].

SNR is a critical metric in signal measurement, including MT signals. A higher SNR value indicates that the signal has relatively low noise compared to a clean signal [53], if the SNR value is low, particularly below 15 dB, it suggests that the signal contains significant noise, making it susceptible to bias and misinterpretation [54]. The calculation of the SNR value can be performed using Equation 3.

$$SNR = 10\ log_{10} \frac{\sum_{i=1}^{N} x_i^2}{\sum_{i=1}^{N} (x_i - y_i)^2} (dB) \tag{3}$$

where x_i represents the original signal value (clean signal), y_i denotes the denoised signal value (predicted result), and (N) is the total number of samples in the signal. After evaluating the model's performance using SNR to measure the comparison between the clean signal and noise, the model is further assessed using NMSE as an additional evaluation metric.NMSE provides a more specific measure of the model's ability to reconstruct a noise-contaminated signal. It evaluates the error between the true value and the value predicted by the model, considering the scale of the data used. Unlike other error metrics, NMSE normalizes the error based on the range of the original data (maximum and minimum values), offering a fairer evaluation when the data has varying scales [55]. The NMSE value can be calculated using Equation 4.

$$\text{NMSE} = \frac{\sum_{i=1}^{N} (y_i - x_i)/N}{x_{max} - x_{min}} \tag{4}$$

where x_{max} and x_{min} are the maximum and minimum values of the original data. After evaluating the model performance using NMSE to determine the signal reconstruction error based on the data scale, the next step is to assess the relationship between the original and denoised signals using the correlation coefficient. NMSE provides an indication of how far the model's predictions deviate from the original signal, whereas the correlation coefficient evaluates how well the original signal pattern is preserved. The correlation coefficient is a statistical measure that describes the strength and direction of the relationship between two variables, ranging from -1 to 1. A value of 1 indicates a perfect positive correlation, -1 indicates a perfect negative correlation, and 0 indicates no correlation. The correlation coefficient can serve as an evaluation metric by illustrating how accurately the model predicts the actual condition. A higher correlation coefficient signifies a better fit, meaning the prediction model is more accurate. The correlation coefficient value can be calculated using Equation 5 [47].

$$Correlation\ coefficient\ = \frac{\sum_{i=1}^{N} (x_i - \bar{y})(y_i - \bar{y})}{\sqrt{\sum_{i=1}^{N} (x_i - \bar{x})^2 \sum_{i=1}^{N} (y_i - \bar{y})^2}} \tag{5}$$

where $\bar{x}$ represents the average original signal, $\bar{y}$ denotes the average predicted signal (after denoising). By using these three metrics, a clearer understanding of the model's effectiveness in removing noise without altering the original structure of the signal can be obtained [37].

3. Results and Discussion

CNN and LSTM algorithms have been used in the same MT signal source, including all electrical and magnetic channels. If, in CNN algorithm application the MT signal is denoised based on the convolutional pattern in the signal processing, in the LSTM the denoising process is fundamentally based on capturing temporal dependencies and patterns from sequential data. So, these two algorithms are learning the pattern of the signal to recognize the MT noise signal and preserving representative signal data when it is appropriate with clean MT signal characteristics.

MT signal denoising from CNN and LSTM are resulting denoised MT signal models from each MT channels and performance metrics, such as Signal-to-Noise Ratio (SNR); Normalized Mean Square Error (NMSE); and correlation coefficient. The denoised MT signal models show the product of machine learning algorithms that have been used to reduce electromagnetic noise. Performance metrics are needed to assess the effectiveness of both models in reducing noise while preserving the original structure of the signal. This research analyses the denoising effect on MT signal model from each machine learning algorithm, also assessing the efficiency of the two models based on training time comparison [56, 57].

3.1. CNN Model Denoising Result

CNN algorithm for MT signal denoising works well and properly, resulting new predicted signal model as denoised MT signal model for each channel. From electrical field in x-axis (Ex) that shown in Figure 7; electrical field in y-axis (Ey) that illustrates in Figure 8; magnetic field in x-axis (Hx) that depicted in Figure 9; magnetic field in y-axis (Hy) that shown in Figure 10; and magnetic field in z-axis (Hz) that illustrated in Figure 11 indicates the similar trend in their signal denoising process. The visualization from each model shows the signal spikes are indicated as noise signal has been diminished by predicting the "normalized" signal trend based on other signal patterns with minimum spikes [26].

CNN model application for MT signal denoising works effectively in removing noise on each channel. The noise signal in the original signal is significantly reduced in the denoised signal model. There is reduction of the sharp fluctuations and irregularities signal that be expected as noise signal. In addition, after the denoising result is overlaid with the original data, the main structure of the original signal is preserved after the denoising process. From this analysis, the denoising process using CNN Algorithm does not change the actual signal information. In detail, MT signal denoising identification by zooming in the signal model, the CNN model is preserving the shape of original signal and effectively removing noise signal indication [27].

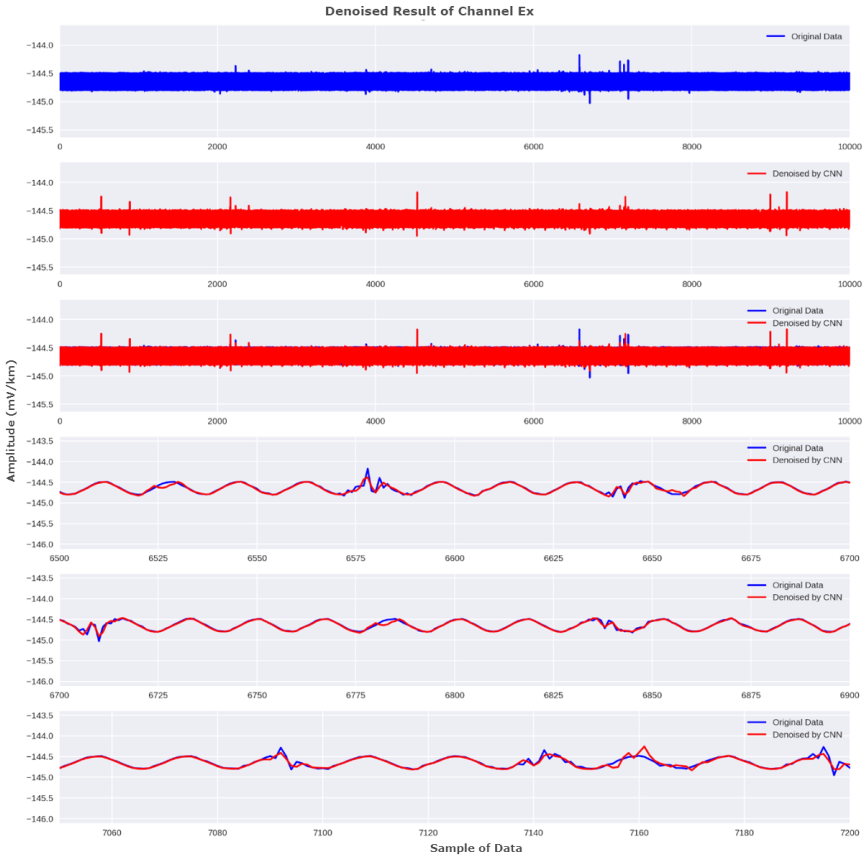

Figure 7. Electric Field Component in X-Axis (Ex) Signal Denoising from CNN Algorithm Application

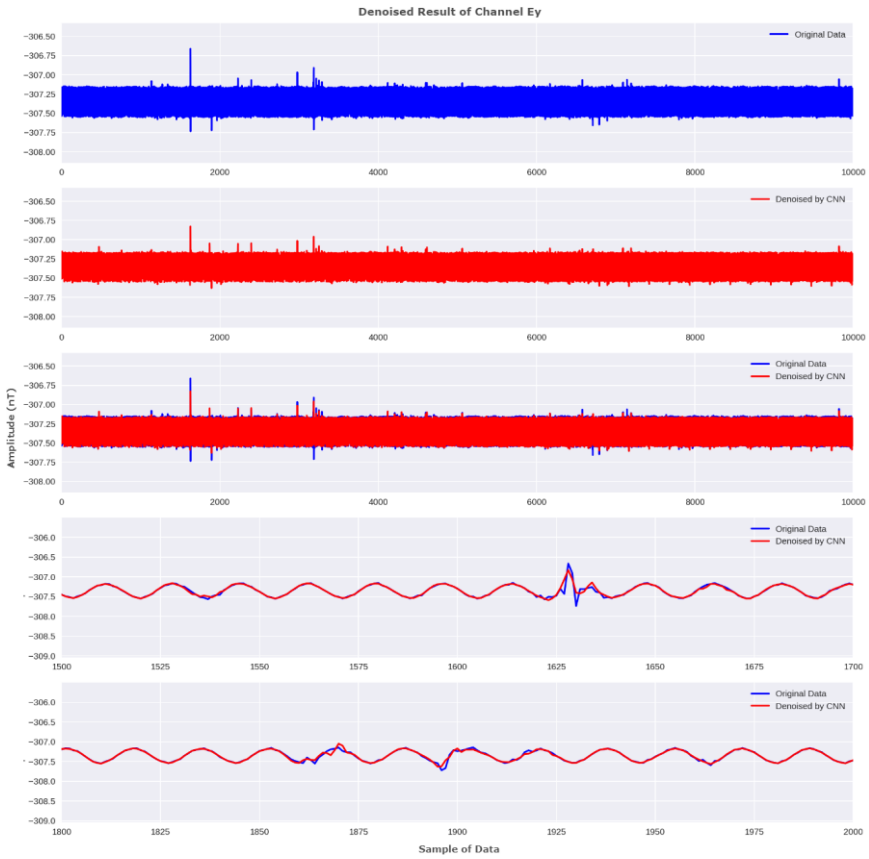

Figure 8. Electric Field Component in Y-Axis (Ey) Signal Denoising from CNN Algorithm Application

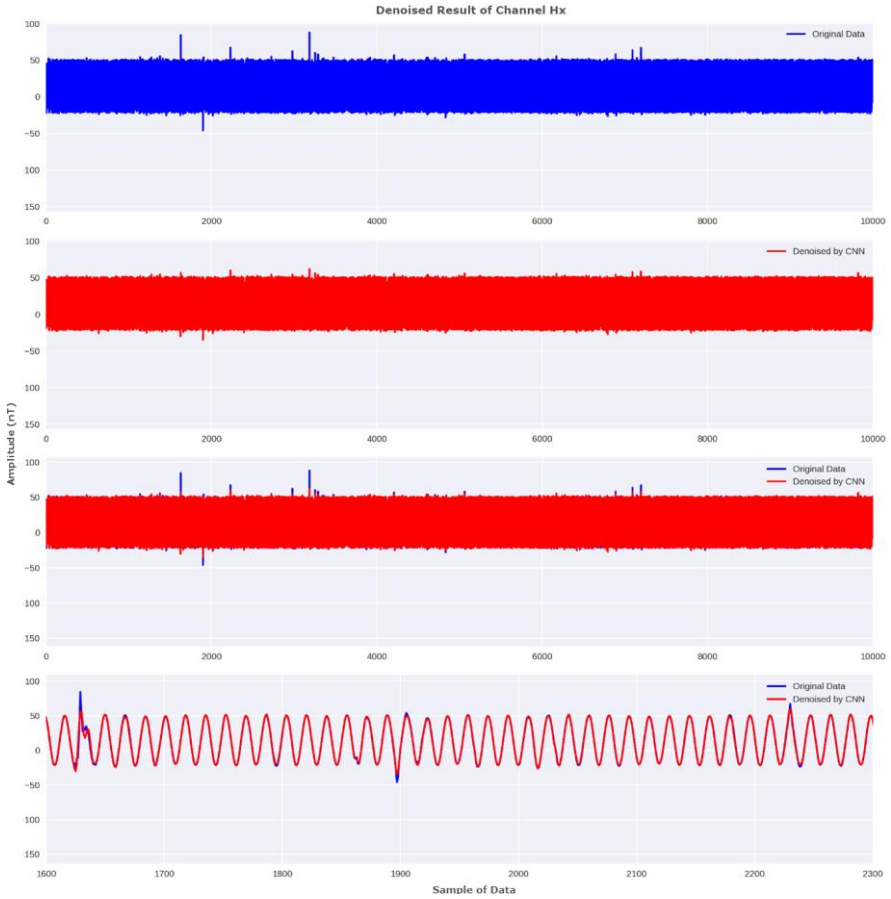

Figure 9. Magnetic Field Component in X-Axis (Hx) Signal Denoising from CNN Algorithm Application

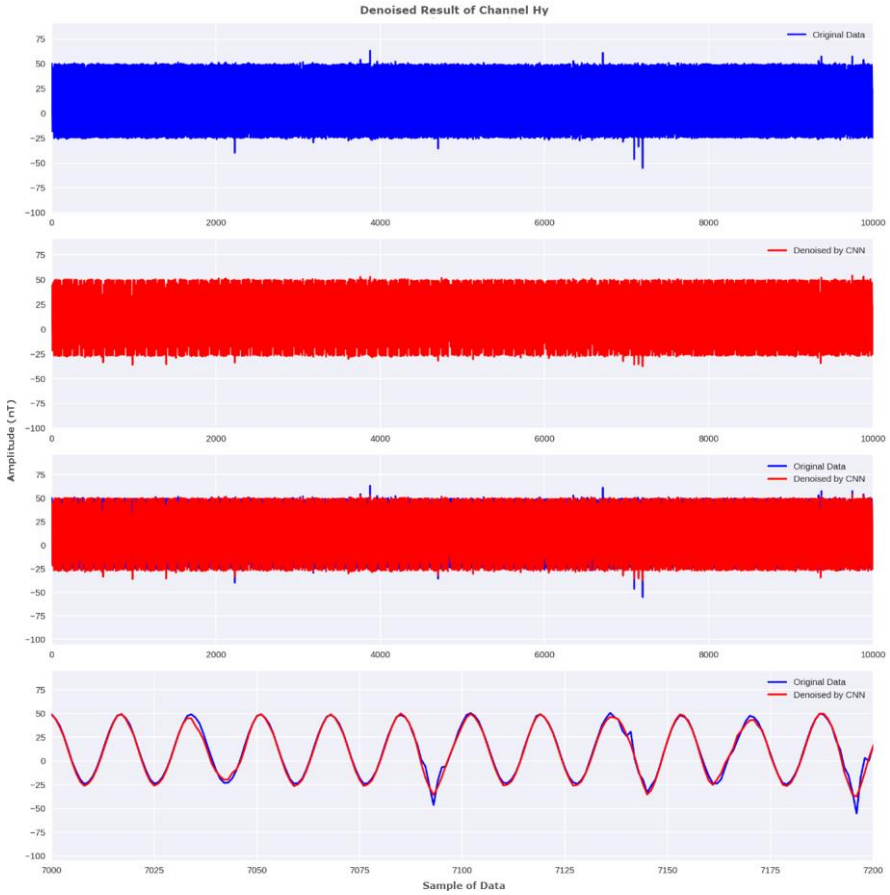

Figure 10. Magnetic Field Component in Y-Axis (Hy) Signal Denoising from CNN Algorithm Application

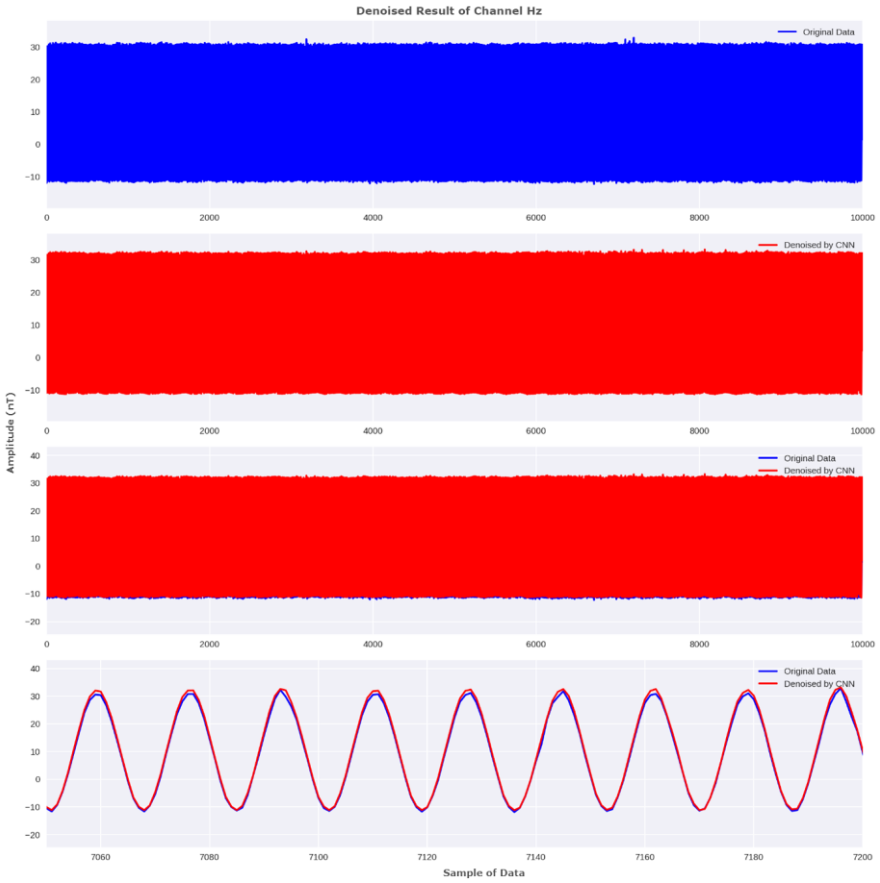

Figure 11. Magnetic Field Component in Z-Axis (Hz) Signal Denoising from CNN Algorithm Application

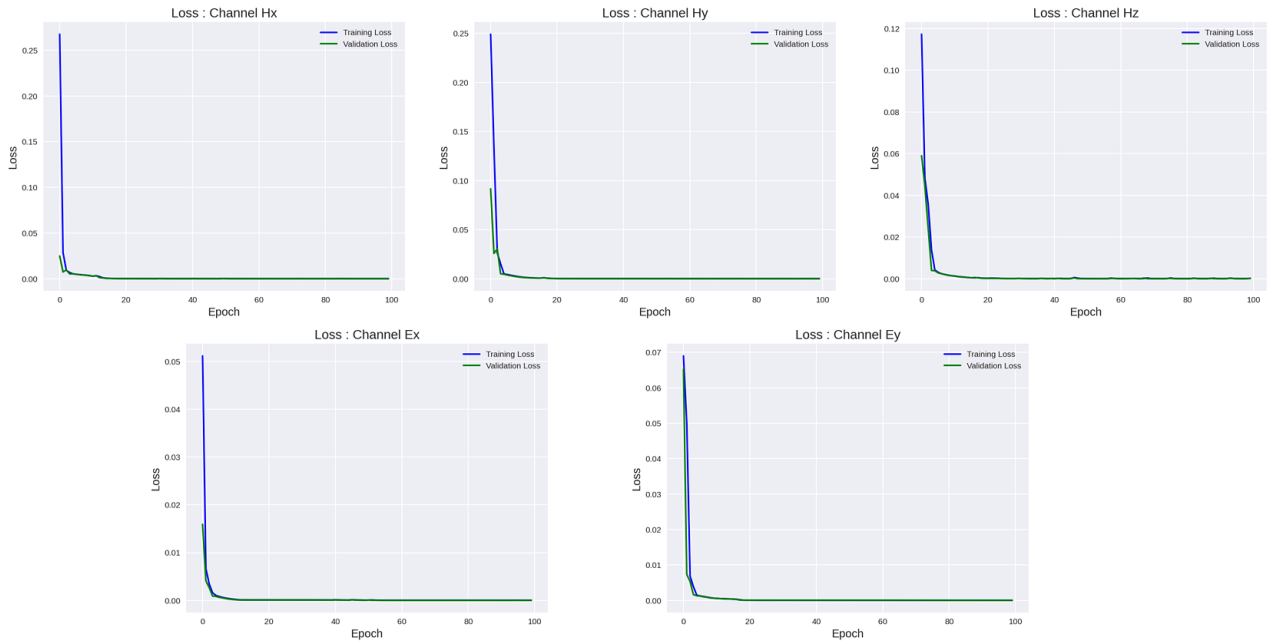

Figure 12. Training and Validation Loss Curve from CNN Algorithm Denoising

CNN model shows optimal performance without any indication of overfitting or underfitting. This indication is known based on loss-epochs diagram for each channel (Ex, Ey, Hx, Hy, Hz), as shows in Figure 12. Training and validation loss significantly decreased in the early epochs, giving an indication if the model learned the data patterns well. After a few epochs, the loss curves became more stable and converged to very low numbers, indicating the model successfully minimized the prediction error. The relationship between the training and validation loss illustrates an insignificant difference between the two curves. The denoised MT signal model did not have any overfitting and underfitting result. It is meaning the model is specifically suitable for training data, did not had any over-generalization in signal denoising process, and able to preserve important patterns from the signal data [58].

Based on Signal-to-Noise Ratio (SNR) analysis, the CNN model is giving significant improvement to the quality of the MT signal and effectively reduced the noise signal. MT signal denoising using CNN algorithm shows an increase in SNR for all channels. In general, the initial SNR has a range of 23.89 to 28.60 dB and increases to 30.74 to 46.76 dB, as shown in Table 4. Figure 13 illustrates that the distribution of SNR value for each channel has a relatively consistent trend of increasing. The most significant SNR value increase has happened to Ex channel, where the SNR increased from 24.58 dB to 43.71 dB, it increased 1.78 times rather than initial SNR. This is followed by Hy channel as second highest SNR value improvement, this channel increasing 1.63 times from 28.60 dB to 46.76 dB. The least increase happened in Hz channel, where it is increased from 24.42 to 30.74 dB, or 1.26 times higher than its initial value [57].

This CNN algorithm for MT signal denoising is resulting in line analysis with the previous research that shows an increase in SNR using machine learning algorithm, that related to effectiveness in its pattern recognition to predict the "normal" signal trend based on surround signal with less spike trend. High SNR indicates low noise in the signal and successful of denoising performance. Thus, the CNN model that has been built in this research is able to remove noise efficiently, resulting in a cleaner and more reliable MT signal [57, 59].

Table 4. Comparison of Initial and CNN-Denoised SNR Across Channels

Channel	SNR (dB)	
	Initial	CNN
Ex	24.58	43.71
Ey	23.89	36.50
Hx	26.71	42.42
Hy	28.60	46.76
Hz	24.42	30.74

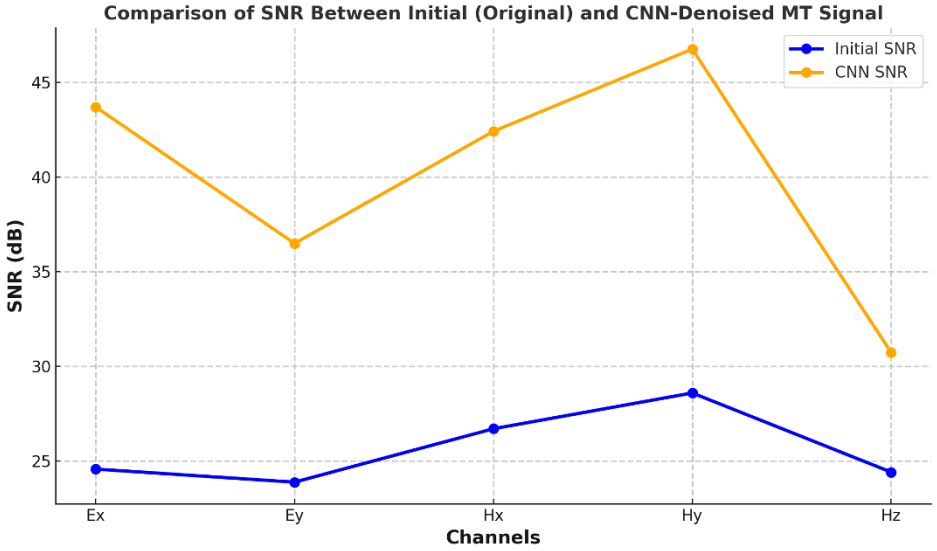

Figure 13. Comparison of SNR between Initial and CNN-Denoised MT Signal

Model performance evaluation from CNN algorithm application in MT signal denoising is carried out using correlation coefficient and NMSE analysis. This evaluation is needed to analyse the effectiveness of denoising using the CNN model. The correlation coefficient and NMSE values are used to assess and illustrate the ability of the denoised MT signal model to maintain the original structure of the signal, simultaneously minimizing the calcuated error after the denoising process. The evaluation results based on these metrics that are presented in Table 5 and Figure 14 [59].

Table 5. Evaluation Metrics of CNN Denoising Result for each Channel

Channel	CNN Model Result Evaluation Metrics	
	Correlation coefficient	NMSE
Ex	0.955	0.006
Ey	0.970	0.014
Hx	0.997	0.007
Hy	0.993	0.006
Hz	0.999	0.033

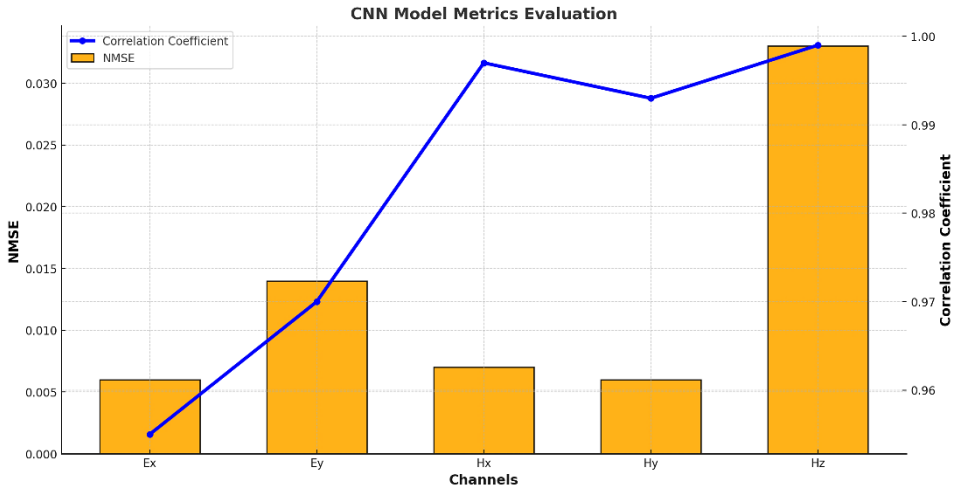

Figure 14. Evaluation of CNN Denoising Performance using Correlation Coefficient and NMSE Across Channels

Denoising model evaluation from CNN algorithm based on the correlation coefficient and NMSE values shows excellent performance, where all channels have a relatively high correlation to the original data. For correlation coefficient, Hz and Hx channels record the highest values of 0.999 and 0.997, respectively. It highlights the CNN algorithm ability to maintain the original signal structure, resulting a good representative signal model. With the range of 0.955 to 0.999, the correlation coefficient indicated whether the denoised signal

was similar to the original signal. A high correlation coefficient value ensures important information in the MT signal is preserved during the denoising process, while noise is successfully reducing the noise without corrupting the original signal pattern [27].

For NMSE evaluation, low NMSE value is related to good representative signal models. The NMSE concept in this evaluation is fundamentally opposite with correlation coefficient. While the correlation coefficient finds the similarity between denoised signal model and the representative of zero-noise signal model, NMSE finds the difference between them. So, NMSE in this research is designed to calculate the error between original and predicted signals, which is identified had relatively low error after the normalization process. The NMSE from CNN algorithm's signal denoising in this research resulted in the value ranges from 0.006 to 0.033, with the Ex and Hy channels having the lowest NMSE of 0.006, reflecting the minimal error after the denoising process. However, the Hz channel, which had the highest correlation coefficient value, is recorded with the highest NMSE of 0.033. Even though, the Hz channel's NMSE is still within the range indicating a relatively low value of error. Based on these evaluation metrics, it is shown that the denoising architecture from CNN algorithm in this research is appropriate and reliable to be used in MT signal processing applications [33].

3.2. LSTM Model Denoising Result

Visual analysis of the LSTM algorithm modelling was successfully reduce the electromagnetic noise for all channels and preserved the important characteristics of the original signal. There is similarity between denoising results with assumed clean MT signal from the original signal, especially in segments with repetitive patterns and uniformed high amplitude. This result indicates that the LSTM algorithm is reliable in improving the quality of MT signals by reducing the noise signal influence on the original MT signal trend [57].

The denoised signal model of electrical field components in x-axis (Ex) and y-axis (Ey) are shown in Figures 15 and 16, respectively. For magnetic field components, the denoised signal model in x-axis (Hx), y-axis (Hy), and z-axis (Hz) are depicted in Figures 17 to 19, respectively. The LSTM denoising results that shown in Figures 15 to 19 sequentially illustrate the original signal diagram, denoised signal diagram using LSTM, overlay of the original signal and the denoising result, and enlarged zoom in of a selected overlay segment to provide more detailed insights into the signal matching between the original signal and the denoising result [44].

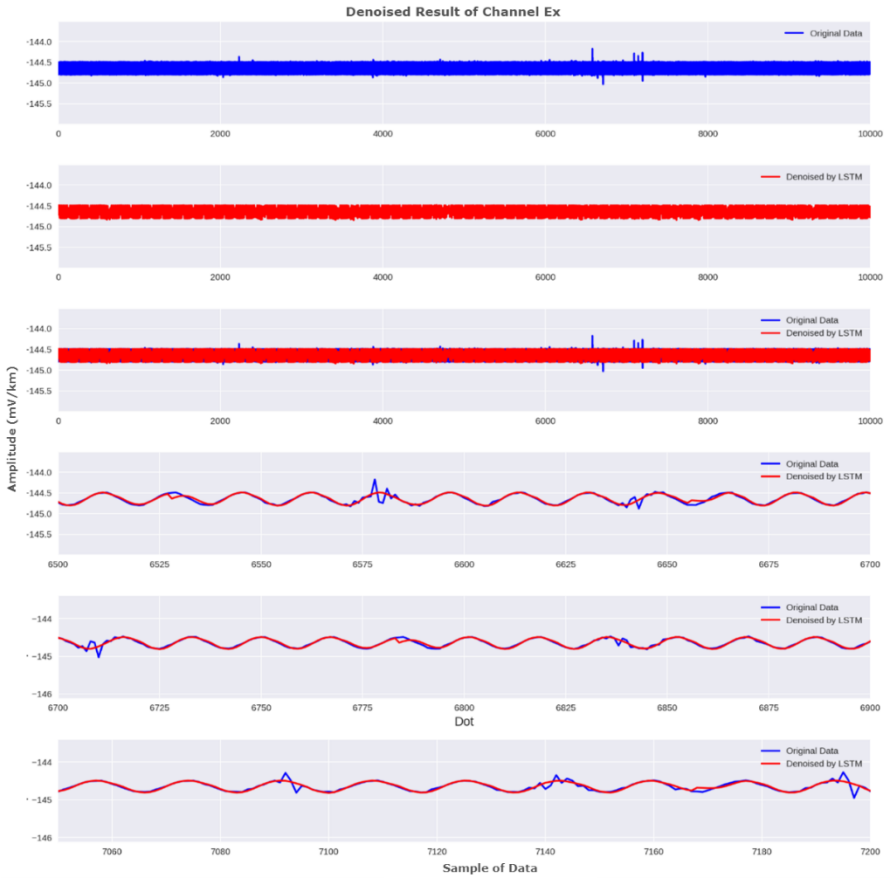

Figure 15. Electric Field Component in X-Axis (Ex) Signal Denoising from LSTM Algorithm Application

Figure 16. Electric Field Component in Y-Axis (Ey) Signal Denoising from LSTM Algorithm Application

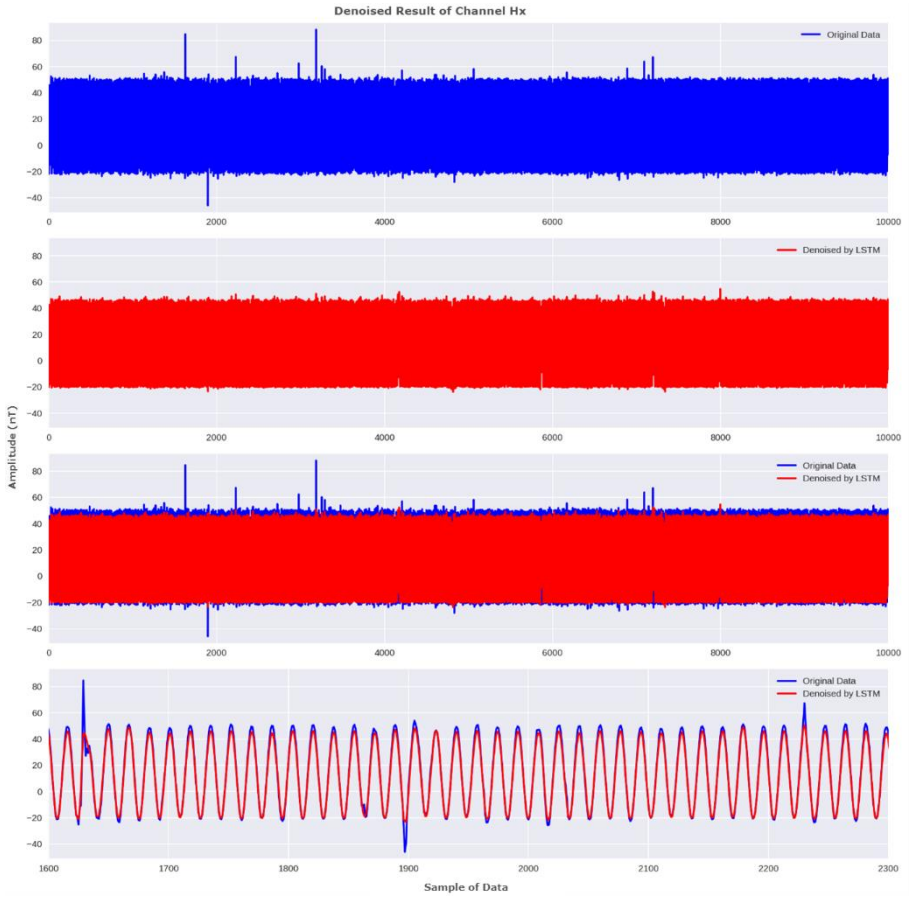

Figure 17. Magnetic Field Component in X-Axis (Hx) Signal Denoising from LSTM Algorithm Application

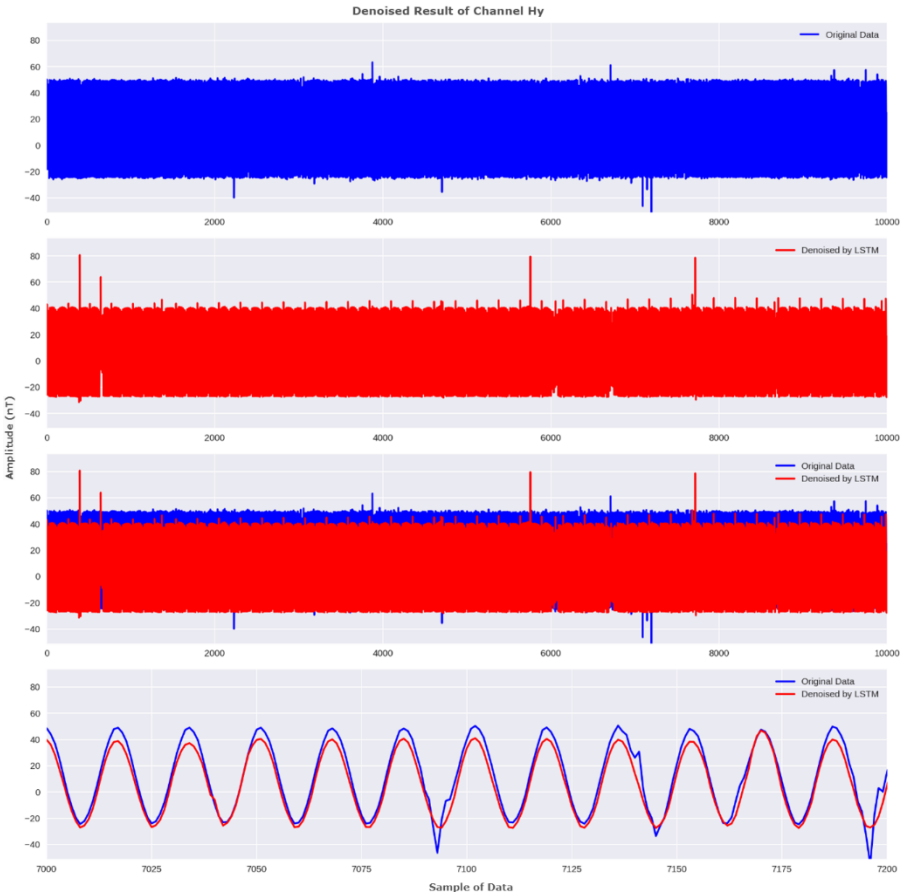

Figure 18. Magnetic Field Component in Y-Axis (Hy) Signal Denoising from LSTM Algorithm Application

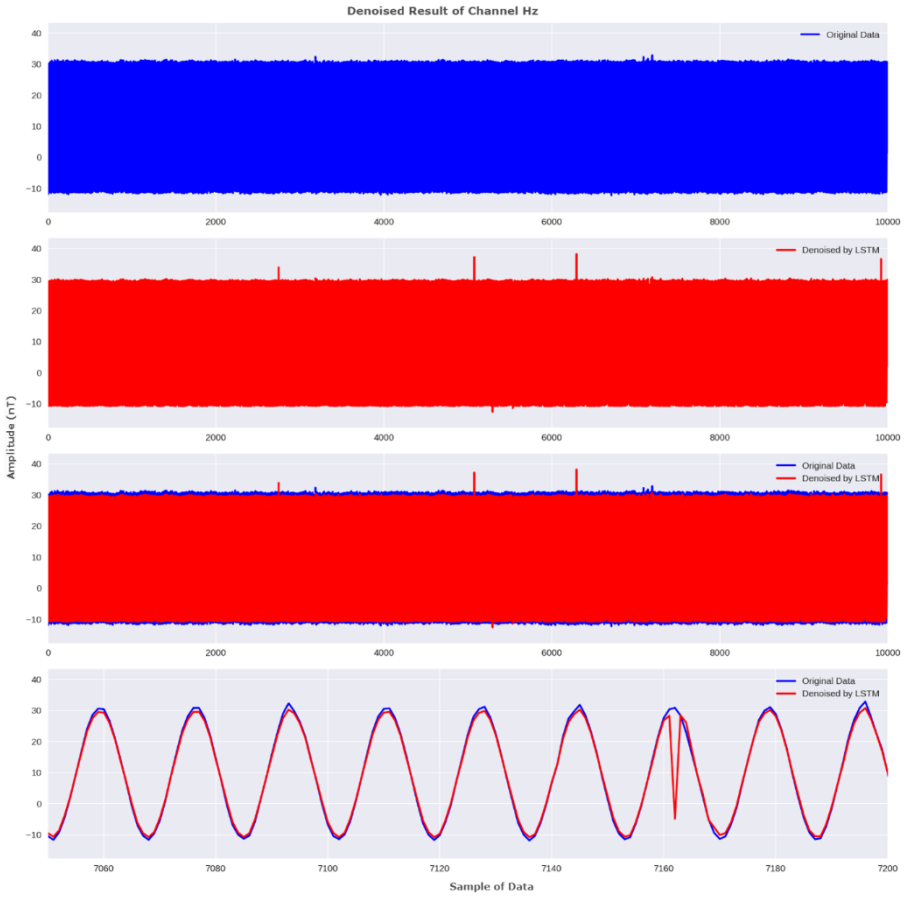

Figure 19. Magnetic Field Component in Z-Axis (Hz) Signal Denoising from LSTM Algorithm Application

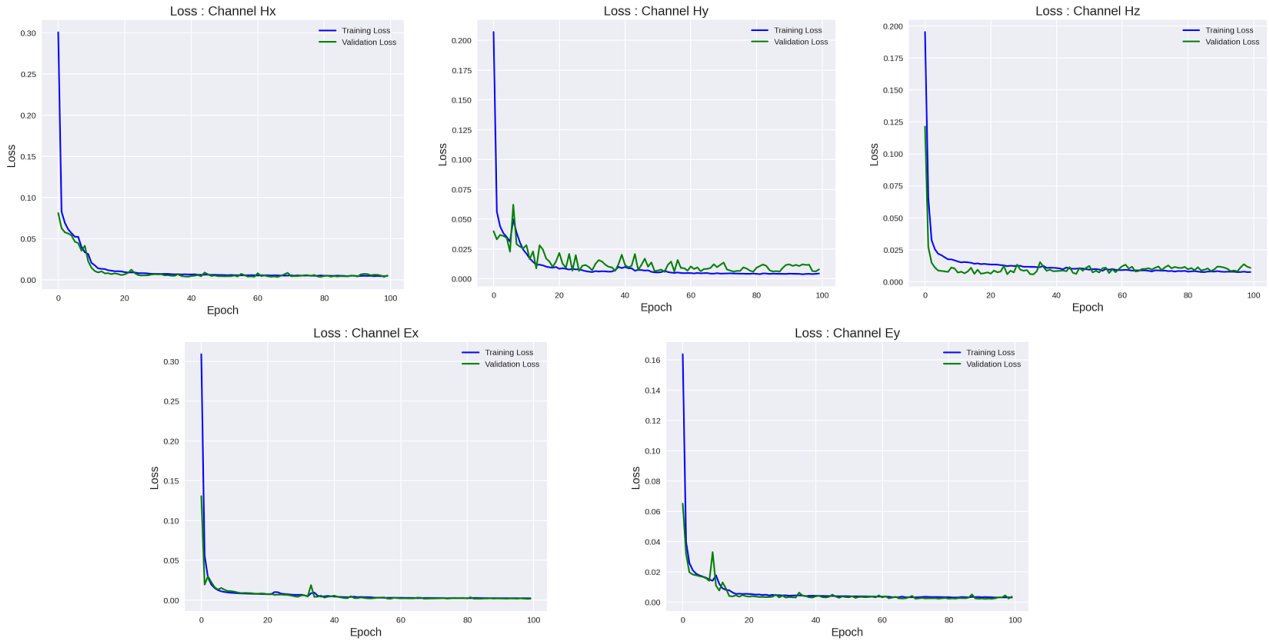

Figure 20. Training and Validation Loss Curve from LSTM Algorithm Denoising

A significant decrease in loss values in the first few epochs is indicating the LSTM algorithm learn the signal data patterns very quickly in this epoch. After reaching low values, both training and validation loss remain stable until the end of the training process. When the training process is running, there are no signs of overfitting or underfitting happened on the loss function analysis. It indicates the analysis not only understands the training data, but also able to perform well on the validation data. There is a consistent trend for all channels that contained a fluctuation at the beginning of training, specifically in the transition of first phase of signal pattern learning and the end of learning. These results show that the model has good generalization ability, where it is very effective in reducing noise and preserves the important structure of the MT signal. Figure 20 illustrates the training and validation loss curve for the LSTM algorithm in MT signal denoising [35].

Denoising results of the LSTM model show significant capability in increasing SNR values for all MT signal channels. Overall, the SNR value has increased from the range of 23.89 to 28.60 dB in the original signal into the range of 30.05 to 41.80 dB after the signal denoising process finished. Ex channel shows the highest SNR increased by 70.1% (1.70 times) from 24.58 dB in the original signal to 41.80 dB after denoising using LSTM, while Ey channel had increased by 44.6%; the Hx channel had increased by 36.9%; Hy channel had increased of 26.5%; and Hz channel had increased of 23%. This improvement shows significant noise reduction in all channels, with a consistent increase trend for all channels' SNR. It indicates that the LSTM effectively reduces noise while maintaining the important characteristics of the original signal. Initial and Denoised SNR from LSTM algorithm modelling was written in Table 6, and its distribution is illustrated in Figure 21 [27].

Table 6. Comparison of Initial and LSTM-Denoised SNR Across Channels

Channel	SNR (dB)	
	Initial	LSTM
Ex	24.58	41.80
Ey	23.89	34.54
Hx	26.71	36.58
Hy	28.60	36.18
Hz	24.42	30.05

Performance evaluation of MT signal denoising by LSTM algorithm is using correlation coefficient and NMSE metrics. These two-evaluation metrics provide deeper analysis related to model's ability to preserve the original signal structure and error rate in the denoising process. These evaluation results are important to understand significance of LSTM algorithm in maintaining data integrity and its effectiveness in reducing electromagnetic signal noise. LSTM model performance for MT signal denoising shows good results, where the correlation coefficient reaches the highest value in the Hz channel (0.999) and the lowest value in the Ex-channel (0.928). It is indicating the ability of LSTM algorithm to maintain the original structure of the signal is reliable and well-performed, especially in the Hz channel.

The sequential approach of LSTM algorithm can be enhanced with some improvement in bidirectional layers to advance unstructured noise, but it will be affecting the longer computation time in process, where it needs the further research to know well about that option [60].

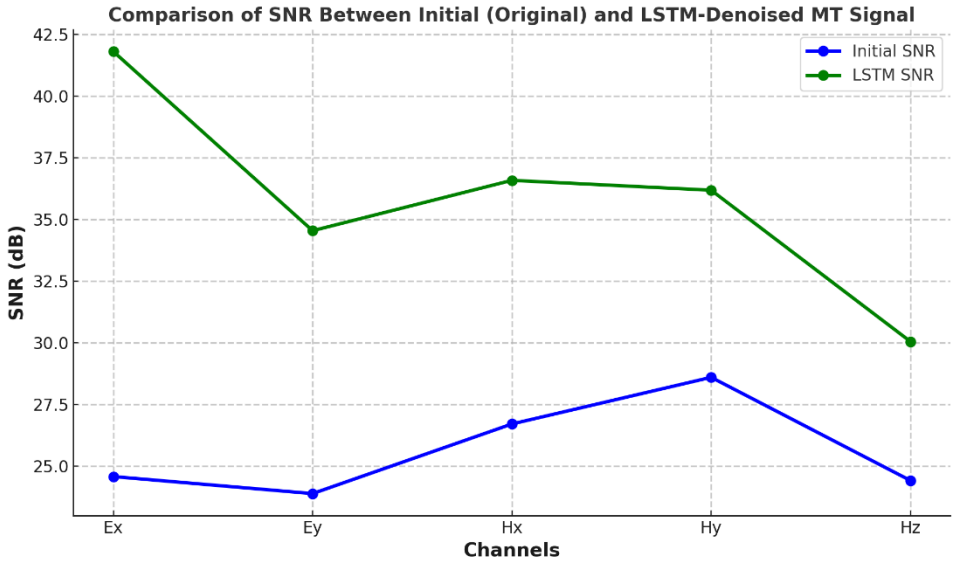

Figure 21. Comparison of SNR between Initial and LSTM-Denoised MT Signal

In LSTM algorithm for MT signal denoising, there are NMSE values range from 0.006 to 0.033. Ex had the lowest NMSE value of 0.008, representing the minimal error in the denoising process. Hz channel is noted to have the highest correlation coefficient value of 0.036, while it still has a relatively low error value. These evaluation metrics illustrate that the denoising architecture from LSTM algorithm in this research is appropriate and reliable to be used in MT signal processing applications. Table 7 written LSTM algorithm evaluation metrics, while Figure 22 illustrates the evaluation metrics distribution in diagram [57].

Table 7. Evaluation Metrics for LSTM Denoising Results on Each Channel

Channel	LSTM model result evaluation metrics	
	Correlation coefficient	NMSE
Ex	0.928	0.008
Ey	0.963	0.019
Hx	0.994	0.015
Hy	0.984	0.016
Hz	0.999	0.036

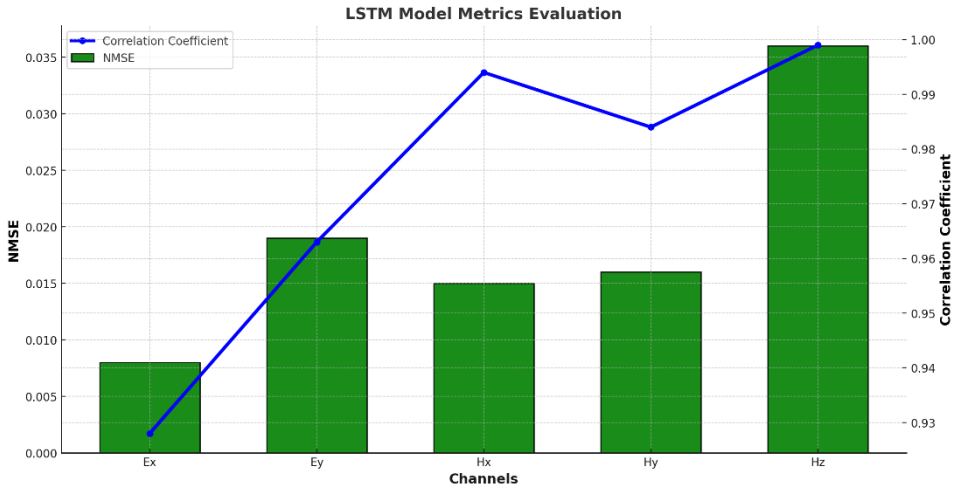

Figure 22. Evaluation of LSTM Denoising Performance using Correlation Coefficient and NMSE Across Channels

3.3. Discussion

After the analysis of each machine learning algorithm, this section will discuss about the results comparison, both in its qualitative and quantitative analysis. The qualitative comparison analysis discusses about the visualization models and the shape of MT signal. Although the denoised MT signal product from CNN and LSTM algorithms had similar forms, but there are several detailed signal's spike that contributes to performance evaluation metrics quantitative. The quantitative comparison analysis will be focused on discussing about the performance evaluation metrics and its distribution value diagrams [44].

In-depth performance analysis of the MT signal denoising model will be focused on two main evaluation aspects: effectiveness and efficiency. Effectiveness is assessed using the performance metrics of SNR, correlation coefficient, and NMSE. Effectiveness describes the model's ability to remove noise while preserving the original signal structure. Efficiency will focus on the computational time required by the model to complete the denoising process. Combination of effectiveness and efficiency analysis represents more comprehensive understanding of each denoising algorithm’s reliability in MT signal processing applications [17].

Signal-to-Noise Ratio (SNR) in this research plays an important role in representing MT signal quality level, both original signal and denoised signal. CNN and LSTM algorithm successfully applied and gave significant result in MT signal denoising. Based on its SNR values enhancement in all MT channel, all denoised MT signal resulting higher SNR than the original one. It indicates both algorithms promise signal enhancement due to its pattern analysis ability in predicting signal noise indication and preserving the real signal data [57].

CNN and LSTM algorithms consistently increase the SNR across various channels compared to the original data. For the CNN algorithm, the improvement of SNR value ranges from 6.32 dB to 18.16 dB, where the denoised MT signal produced SNR value in the range of 1.3 to 1.6 times higher than the original one. This range highlights CNN's effectiveness in denoising MT signals, with the best performance observed in the Hy channel, which recorded the highest SNR value increase of 18.16 dB; from 28.60 dB (initial signal) to 46.76 dB (after CNN denoising) representing an increase of 1.6 times higher. LSTM algorithm for MT signal denoising also illustrates the SNR value enhancement, while it is resulting in slightly inferior improvement rather than CNN's result. The SNR enhancement in the LSTM algorithm application varies from 5.63 dB to 9.83 dB, where it is equivalent to a 1.2 to 1.4 times increment. The SNR value comparison has been written in Table 8, and its value distribution is depicted in Figure 23 [27].

SNR values distribution that compares original value, denoised CNN value, and denoised LSTM value show the superiority of CNN algorithm to enhance SNR value in MT signal denoising, rather than LSTM algorithm application. In SNR values distribution in Figure 23, it is illustrating all electrical and magnetic channel of MT signal data is dominated by CNN algorithm results. It can be interpreted if the convolutional layer pattern analysis in CNN algorithm works better than temporal dependencies from sequential patterns analysis in LSTM in denoising MT signal [27].

In deeper analysis, CNN algorithm is resulting better MT signal quality enhancement rather than LSTM algorithm in the magnetic field channels, while in the electrical field channels, those algorithms show an identical trend. It is an indication if the magnetic field signal in the MT survey is more appropriate in using the CNN algorithm as a denoising signal filter rather than the LSTM algorithm. However, in the electrical field signal, both of algorithms have similar improvements, but CNN is promising a slightly better denoised signal [26].

Both CNN and LSTM algorithms show their best performance on the Ex-channel, with significantly higher SNR values compared to other channels after the denoising process. This indicates that both methods are highly effective in removing signal noise and reconstructing the denoised signal at this channel. Based on information in Table 8 and Figure 23, the CNN algorithm is increasing the SNR value from 24.58 dB to 43.17 dB. It is equivalent to 75.63% or 1.76 times higher than the original one. Besides, LSTM improves the SNR value from 24.58 dB to 41.80 dB, where it represents improvement of 70.05% or 1.70 times higher than the original one [34].

The most significant difference SNR improvement happened in Hy channel. The CNN algorithm's result is gaining the SNR value from 28.60 dB to 46.76 dB, where it is increased by 63.49% or 1.63 times higher. It is making huge difference with SNR value enhancement from LSTM algorithm application, where only increased from 28.60 dB to 36.18 dB. It is just improved 26.50% or 1.26 times higher than SNR value from the original signal [17].

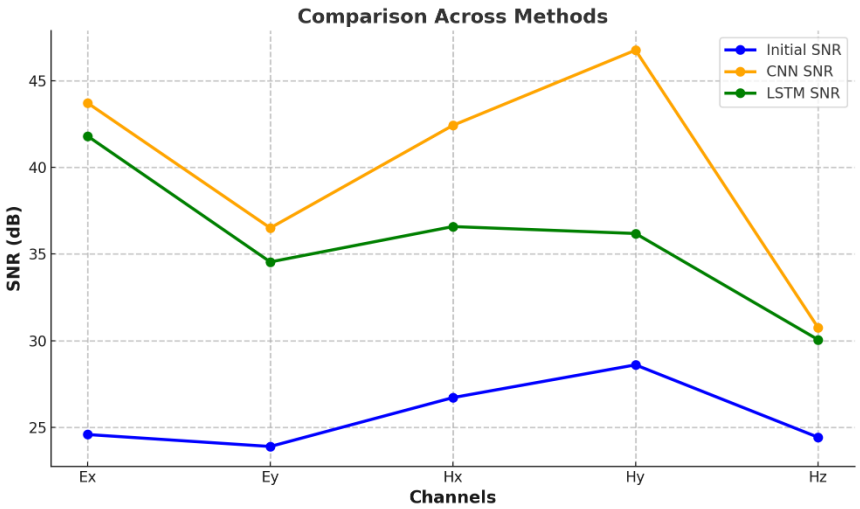

Figure 23. Comparison of SNR Across Initial, CNN, and LSTM Methods

Table 8. SNR Comparison: Initial, CNN, and LSTM Denoised Signals

Channel	SNR (dB)		
	Initial	**CNN**	**LSTM**
Ex	24.58	**43.71**	41.80
Ey	23.89	**36.50**	34.54
Hx	26.71	**42.42**	36.58
Hy	28.60	**46.76**	36.18
Hz	24.42	**30.74**	30.05

For the qualitative analysis based on the signal model, the Hx channel consistently shows significant denoising performance, which can be attributed to the structured signal patterns. These patterns predominantly consist of clear and stable recurring amplitudes, as illustrated in Figure 24. Moreover, the noise on the Hx channel tends to be localized, sporadic, irregular, and characterized by infrequent fluctuations. These characteristics made the noise easier to identify and simplify in the denoising process [36].

Otherwise, the Hz channel became the most challenging MT channel to denoise using both methods. CNN increases the SNR value from 24.42 dB to 30.74 dB, while LSTM improves the SNR value from 24.42 dB to 30.05 dB. The challenge in denoising the Hz channel is caused by more evenly distributed noise with constant and smooth amplitude compared to other channels. The noise signal amplitude does not illustrate significant fluctuations and remains relatively smooth, as illustrated in Figure 25 [19].

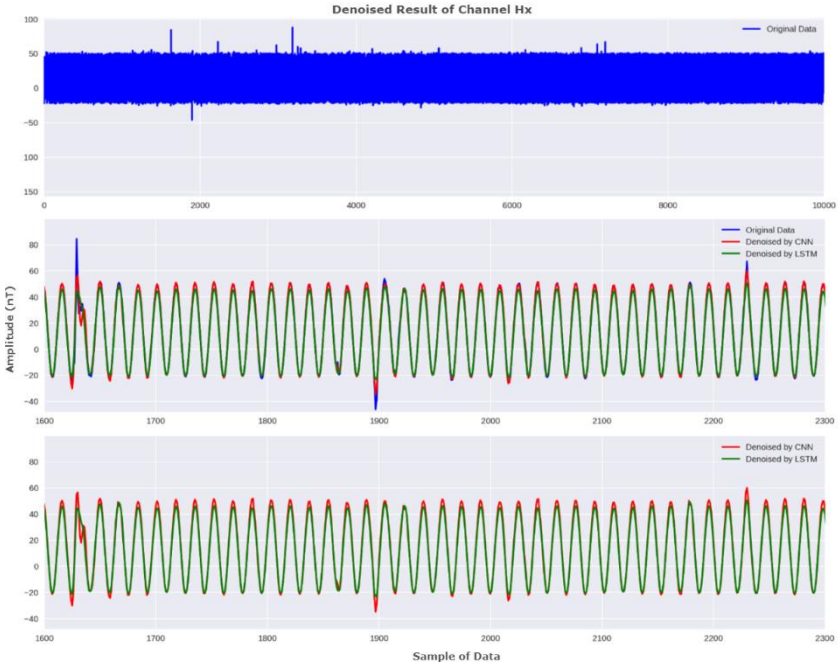

Figure 24. Visualization of MT Signal in Hx Channel

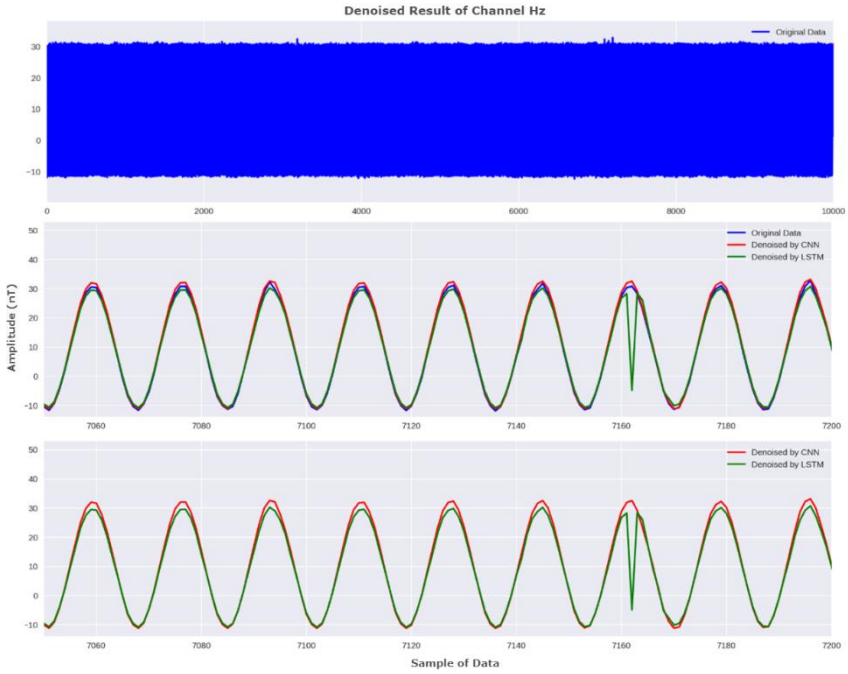

Figure 25. Visualization of MT Signal in Hz Channel

Correlation coefficient and Normalized Mean Square Error (NMSE) are utilized to provide comprehensive performance metrics assessment of the denoising algorithms in this research. While SNR represents the algorithm's ability to enhance signal quality by reducing noise, it does not fully reflect the accuracy level or the errors incurred during the denoising process. Therefore, the correlation coefficient measures how denoised MT signal results preserve the linearity of the original signal patterns, whereas the NMSE is used to evaluate the magnitude of errors relative to the denoised MT signal to the original signal. The combination of these metrics offers a more holistic analysis related to the effectiveness of the denoising process [17].

CNN algorithm consistently overcomes LSTM algorithm in providing better MT signal denoising in this research. Based on the correlation coefficient and NMSE values that are written in Table 9 and illustrate its value distribution diagram in Figure 26, CNN algorithm consistently shows superior performance compared to the LSTM algorithm, with a higher correlation coefficient and lower NMSE values. In the correlation coefficient analysis, CNN algorithm achieves the values in the range of 0.955 to 0.999. It indicates that the CNN algorithm effectively preserves the real signal data to ensure that the essential characteristics of the MT signal remain intact. The LSTM algorithm produces the values in the range of 0.928 to 0.999. It is slightly less than the correlation coefficient's result from CNN algorithm in the Ex channel (0.955 in CNN and 0.928 in LSTM); Ey channel (0.970 in CNN to 0.963 in LSTM); Hx channel (0.997 in CNN and 0.994 in LSTM); and Hy channel (0.993 in CNN and 0.984 in LSTM). The interesting result happened in Hz channel when both CNN and LSTM algorithms had exact same value if 0.999 [26, 35].

For NMSE analysis, CNN algorithm also shows better performance than LSTM algorithm. In general, CNN algorithm had lower NMSE value rather than LSTM algorithm. The CNN algorithm produces the NMSE values in the range of 0.006 to 0.0033; while the LSTM algorithm produces the NMSE values in the range iof 0.008 to 0.036. These values range is relatively low for NMSE, so those two algorithms are producing good denoising signal in this research. The NMSE value's difference among those algorithms in each MT channel is very thin. CNN algorithm products were promising better result with lower NMSE value in Ex channel (0.006 in CNN and 0.008 in LSTM); Ey channel (0.014 in CNN and 0.019 in LSTM); Hx channel (0.007 in CNN and 0.015 in LSTM); Hy channel (0.006 in CNN and 0.016 in LSTM); also Hz channel (0.033 in CNN and 0.036 in LSTM) [61].

Table 9. Comparison of Correlation Coefficient and NMSE Between CNN and LSTM Models Across Channels

Channel	CNN		LSTM	
	Correlation coefficient	NMSE	Correlation coefficient	NMSE
Ex	**0.955**	**0.006**	0.928	0.008
Ey	**0.970**	**0.014**	0.963	0.019
Hx	**0.997**	**0.007**	0.994	0.015
Hy	**0.993**	**0.006**	0.984	0.016
Hz	**0.999**	**0.033**	0.999	0.036

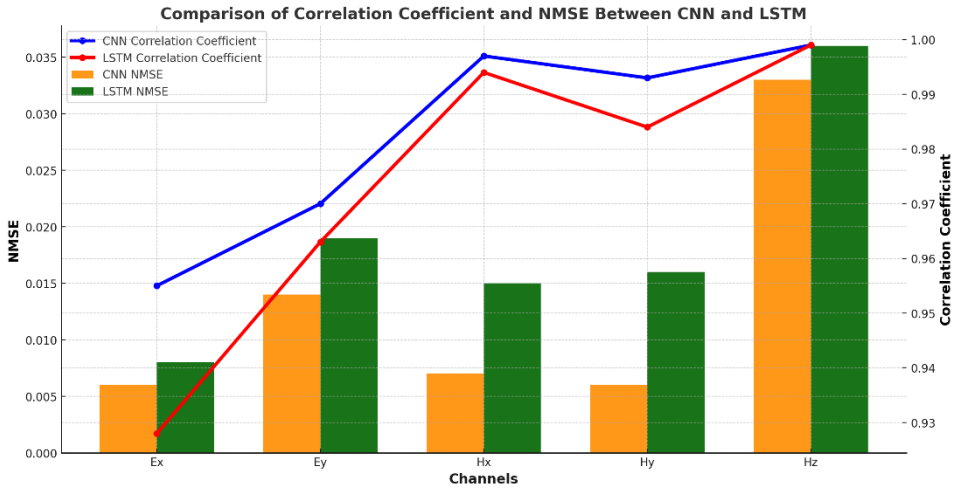

Figure 26. Comparison of Correlation Coefficient and NMSE Metrics Between CNN and LSTM Across All Channels

Correlation coefficient and NMSE values are supporting the SNR analysis in evaluating the denoising results of CNN and LSTM on MT data, if the CNN algorithm promising better performance than LSTM algorithm. The combination of higher correlation coefficients and lower NMSE for CNN algorithm rather than LSTM algorithm, illustrating the effectiveness of CNN algorithm in preserving the real signal structure and promising better signal noise elimination compared to LSTM [27].

The performance of CNN and LSTM algorithms in this research shows clear differences based on the MT signal denoising process characteristics. CNN has proven to be superior with distinct and stable recurring amplitude patterns that are localized, sporadic, irregular, and characterized by infrequent fluctuations. These characteristics are easier to identify, simplifying the denoising process, as they align well with CNN's mechanism, which focuses on local patterns. In contrast, LSTM algorithm faces limitation in handling the electromagnetic noise that is more evenly distributed with constant amplitude. The denoised signal does not result in significant fluctuations and remains smooth. LSTM algorithm in sequential processing gave intention to capture long-term temporal signal patterns and made it less effective for sporadic noise. Furthermore, the lack of temporal structure in MT noise often exacerbates LSTM algorithm performance issues [3].

Processing time is the computation information that potentially influence the machine learning algorithm preference for MT signal denoising. Efficiency evaluation by examining the computational time required by each algorithm for denoising MT data to determine which algorithm provides better efficient computation process. Figure 27 illustrates the comparison of computation times, where CNN algorithm outperforms LSTM algorithm in efficient computation time across all MT channels. CNN algorithm needs 24.83 to 29.16 seconds to process the MT signal denoising, while LSTM algorithm requires 67.38 to 70.69 seconds. It is showed if CNN algorithm has processed MT signal denoising approximately 3 times faster than LSTM algorithm [26].

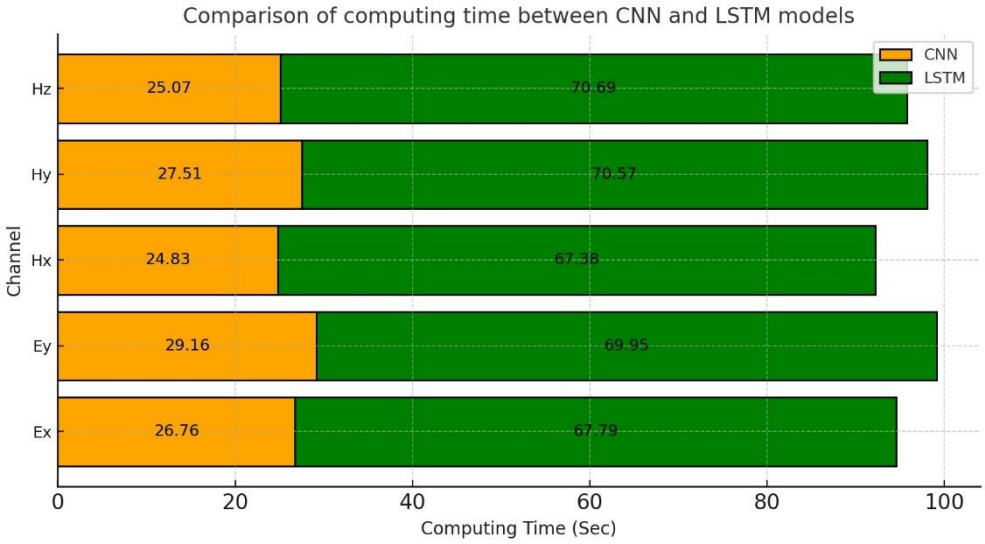

Figure 27. Comparison of Computing Time Between CNN and LSTM Models Across Channels

This computation time difference is caused by CNN algorithm ability to capture local patterns without relying on data sequences, making it highly effective in addressing local and sporadic noise commonly found in MT signal data. It is also supported by CNN algorithm architecture that worked on convolutional layers to detect key patterns in the MT signal data. CNN proves to be more relevant and suitable for denoising tasks on MT signal data. The overall results of the analysis indicate that CNN has a significant advantage over LSTM in denoising MT signal data, both in terms of effectiveness and efficiency [35].

Referring to previous research with similar research methods, this research promises more efficient computation processing time. The CNN algorithm application to denoise MT signal processing previously did in 92 seconds [26]. There is potential if the previous research used larger MT signal dataset and caused the computation processing time longer than CNN algorithm application in this research (24.83 to 29.16 seconds). There is limited information about time processing in LSTM algorithm in MT signal denoising in previous research. With approximately 67.38 to 70.69 seconds in LSTM's denoising algorithm, it is still promising to be used as denoising algorithm in MT signal data. Further challenges will be related to larger and complex MT signal dataset, where the indication is potentially impacting the computation time needed to denoise its MT signal dataset. Larger and more complex MT signal dataset will affect longer computation time, but it is potentially addressed by advance computing devices and efficient computation scripts [61].

This research is potentially developed for other research in geophysics and non-geophysics problems. One-dimension (1D) data like MT signal in this research, is similar to other geophysical data, such as passive seismic and well-log data [62]. Both CNN and LSTM algorithms are potentially used to analyse the potential noise and find the denoising algirthm to improve its data quality. Due to its work's mechanism in recognising data pattern and temporal sequential value distribution, CNN aldn LSTM algorithm is very potential to develop into two-dimensions (2D) and three-dimensions (3D) datasets, where it will be helpful to enhance spatial resolution and reveal potential unidentified feature in geoscience application [24].

4. Conclusions

This study provides in-depth insights into the performance of two deep learning algorithms, CNN and LSTM, in denoising MT data. The evaluation covers effectiveness, efficiency, and the suitability of each method for the data's characteristics, resulting in the following key points:

- Effectiveness — CNN demonstrates superior performance compared to LSTM in denoising MT data, as evidenced by the evaluation metrics. CNN significantly improves SNR, achieves lower NMSE values, and maintains higher correlation coefficients, reflecting its ability to preserve the relationship between the original signal and the denoising results.
- Efficiency — CNN demonstrates computation times that are 2 to 3 times faster than LSTM across all channels for completing the denoising process, making CNN a more resource-efficient choice.
- Alignment with MT Data Characteristics — CNN is more suitable and optimal for handling noise in MT data due to its architecture, which focuses on local patterns without relying on data sequences. This makes it highly effective at addressing local and sporadic noise commonly found in MT data, such as in the Hx and Hy channels, which exhibit stable recurring amplitude patterns, irregular noise, and large but infrequent fluctuations. In contrast, LSTM, with its sequential approach for capturing long-term temporal relationships, is less effective for MT data, which often contains unstructured noise. This is particularly evident in the Hz channel, where noise is evenly distributed with constant amplitude. These characteristics result in LSTM's performance being lower than CNN in denoising MT data.

This experiment demonstrates that CNN is more effective and efficient than LSTM for denoising MT data, achieving significant SNR improvements, low NMSE, higher correlation coefficients, and faster computation times. In the field of geophysics, these results are critical as high-quality MT data supports accurate subsurface exploration and geological mapping. These outcomes provide guidance for geophysics practitioners in selecting the appropriate algorithm while also paving the way for optimizing alternative models or hybrid architectures for more complex geophysical applications in the future.

4.1. Limitations and Post-Study Plan

This research holds significant potential for further development, despite some current limitations, such as the use of a single dataset, computational resource constraints, and the lack of exploration into alternative models that may better align with the data characteristics. Furthermore, the model's evaluation has so far been limited to quantitative metrics such as SNR, NMSE, and correlation coefficient, without incorporating qualitative assessments or testing against more complex noise variations. To address these limitations, future research plans include validating the model on diverse datasets, exploring new model architectures that are more adaptive to noise variations, and applying alternative approaches such as Transformer-based models or hybrid architectures to achieve more optimal results.

Additional studies will also focus on optimizing computational efficiency, testing with supplementary evaluation metrics including qualitative aspects and integrating real-time denoising systems. This research strongly aligns with the Sustainable Development Goals (SDGs), particularly Goal 7 (Affordable and Clean Energy) and Goal 9 (Industry, Innovation, and Infrastructure). By developing effective and efficient denoising models, this study enhances geophysical data analysis, accelerates renewable energy exploration, and drives data-driven technological innovation. The initial success of these models provides a strong foundation for advancing sustainable solutions in the energy and industrial sectors in the future.

5. Declarations

5.1. Author Contributions

Conceptualization, W.U. and D.W. ; methodology, S.A.G., M.U.N.A., A.N.F.I., and D.S.P.; software, M.U.N.A. and A.N.F.I.; validation, W.U. and S.A.G.; formal analysis, W.U., S.A.G., A.N.F.I., and D.S.P.; investigation, A.N.F.I. and D.S.P.; resources, M.U.N.A., A.N.F.I., and D.S.P.; writing—original draft preparation, S.A.G., M.U.N.A., D.S.P., and A.N.F.I.; writing—review and editing, W.U., S.A.G., D.P.N.P., and R.F.I.; visualization, M.U.N.A. and D.S.P.; supervision, W.U., M.H., D.W., and W.L.; project administration, D.S.P.; funding acquisition, W.U. All authors have read and agreed to the published version of the manuscript.

5.2. Data Availability Statement

The data presented in this study are available in the article.

5.3. Funding

The researchers received financial support from Institut Teknologi Sepuluh Nopember (ITS) through the ITS-UTP Batch 2 Partnership Research Scheme in 2024. This research was conducted under the Agreement on the Implementation of the Research Partnership, Contract Number 2107/PKS/ITS/2024.

5.4. Acknowledgments

The authors express their gratitude to Institut Teknologi Sepuluh Nopember (ITS) for the financial support provided through the ITS-UTP Batch 2 Partnership Research Scheme in 2024. The authors also acknowledge Universiti Teknologi Petronas (UTP) for their valuable collaboration as a research partner. Additionally, the authors extend their appreciation to all individuals who contributed to the successful completion of this research project. This study would not have been accomplished without the invaluable contribution of MT data sharing from Dr. Koki Aizawa of SEVO, Kyushu University, who kindly provided the remote reference data for model development. Additionally, we extend our gratitude to Dr. Agnis Triahadini for her significant role in handling the data.

5.5. Institutional Review Board Statement

Not applicable.

5.6. Informed Consent Statement

Not applicable.

5.7. Declaration of Competing Interest

The authors declare that there are no conflicts of interest concerning the publication of this manuscript. Furthermore, all ethical considerations, including plagiarism, informed consent, misconduct, data fabrication and/or falsification, double publication and/or submission, and redundancies have been completely observed by the authors.

6. References

[1] Afshar, A., Norouzi, G. H., & Moradzadeh, A. (2023). Exploring Geothermal Potential through Multi-Modal Geophysical Data Integration: Gravity, Magnetic, and Magnetotelluric Prospecting. International Journal of Mining and Geo-Engineering, 57(4), 427–434. doi:10.22059/ijmge.2023.364057.595093.

[2] Saibi, H., Khosravi, S., Cherkose, B. A., Smirnov, M., Kebede, Y., & Fowler, A. R. (2021). Magnetotelluric data analysis using 2D inversion: A case study from Al-Mubazzarah Geothermal Area (AMGA), Al-Ain, United Arab Emirates. Heliyon, 7(6), e7440. doi:10.1016/j.heliyon.2021.e07440.

[3] Love, J. J., Lucas, G. M., Rigler, E. J., Murphy, B. S., Kelbert, A., & Bedrosian, P. A. (2022). Mapping a Magnetic Superstorm: March 1989 Geoelectric Hazards and Impacts on United States Power Systems. Space Weather, 20(5), e2021SW003030. doi:10.1029/2021SW003030.

[4] Klanica, R., Pek, J., & Hill, G. (2023). Magnetotelluric Power Line Noise Removal Using Temporally Varying Sinusoidal Subtraction of the Grid Utility Frequency. Pure and Applied Geophysics, 180(9), 3303–3317. doi:10.1007/s00024-023-03323-w.

[5] Yun, Z., An, Z., Di, Q., Zhang, Y., Liang, P., Fu, C., Yun, Z., An, Z., Di, Q., Zhang, Y., Liang, P., Fu, C., Yun, Z., An, Z., Di, Q., Zhang, Y., Liang, P., & Fu, C. (2024). Lithospheric electrical structure and geodynamic model of the red river fault zone and its adjacent areas in southwest China: Constraints from 3-D magnetotelluric imaging. Journal of Asian Earth Sciences, 273(June), 106257. doi:10.1016/j.jseaes.2024.106257.

[6] Guo, Z., Han, J., Liu, L., Wu, Y., Hou, J., & Gong, X. (2024). Reducing Reliance on Observation Duration of Magnetotelluric Impedance Estimation with an Improved Instantaneous Spectrum-Based Method. IEEE Transactions on Geoscience and Remote Sensing, 62, 1–15. doi:10.1109/TGRS.2024.3386646.

[7] Balasco, M., Lapenna, V., Rizzo, E., & Telesca, L. (2022). Deep Electrical Resistivity Tomography for Geophysical Investigations: The State of the Art and Future Directions. Geosciences (Switzerland), 12(12), 438. doi:10.3390/geosciences12120438.

[8] Strack, K., Paembonan, A. Y., Davydycheva, S., & Hanstein, T. (2022). An Array Multi-Physics Acquisition System with Focus on Reservoir Monitoring for the Energy Transition. Earth & Environmental Science Research & Reviews, 5(4), 8. doi:10.33140/eesrr.05.04.08.

[9] Triahadini, A., Aizawa, K., Hashimoto, T. M., Chiba, K., Uchida, K., Yamamoto, Y., Miyano, K., Muramatsu, D., Aniya, S., Okubo, A., & Kawamura, Y. (2023). Magma transport along structural boundaries in the upper crust: insights from broad-band magnetotelluric constraints on the structure beneath Unzen volcano, Japan. Geophysical Journal International, 234(2), 1268–1281. doi:10.1093/gji/ggad126.

[10] Zhang, L., Ren, Z., Xiao, X., Tang, J., & Li, G. (2022). Identification and Suppression of Magnetotelluric Noise via a Deep Residual Network. Minerals, 12(6), 766. doi:10.3390/min12060766.

[11] Egbert, G. D. (1997). Robust multiple-station magnetotelluric data processing. Geophysical Journal International, 130(2), 475–496. doi:10.1111/j.1365-246X.1997.tb05663.x.

[12] Clarke, J., Gamble, T. D., Goubau, W. M., Koch, R. H., & Miracky, R. (1983). Remote- reference magnetotellurics: Equipment and procedures. Geophysical Prospecting, 31(1), 149-170.

[13] Usui, Y., Uyeshima, M., Sakanaka, S., Hashimoto, T., Ichiki, M., Kaida, T., Yamaya, Y., Ogawa, Y., Masuda, M., & Akiyama, T. (2024). New robust remote reference estimator using robust multivariate linear regression. Geophysical Journal International, 238(2), 943–959. doi:10.1093/gji/ggae199.

[14] Widodo, A., Lestari, W., Warnana, D. D., Syaifuddin, F., Rivensky, R. S., & Ilmawan, R. Z. (2021). Analysis of the effect of magnetotelluric data quality improvement using rho variance and edit XPR parameters in densely populated areas. IOP Conference Series: Earth and Environmental Science, 851(1), 012003. doi:10.1088/1755-1315/851/1/012003.

[15] Zhan, Q., Liu, Y., Liu, C., & Zhao, P. (2025). A Novel Decomposition-Enhanced Denoising Method for Magnetotelluric Data Based on AMSE-REWT in the Time–Frequency Domain. IEEE Transactions on Geoscience and Remote Sensing, 63. doi:10.1109/TGRS.2025.3531497.

[16] Zhou, R., Han, J., Guo, Z., & Li, T. (2021). De-noising of magnetotelluric signals by discrete wavelet transform and SVD decomposition. Remote Sensing, 13(23), 4932. doi:10.3390/rs13234932.

[17] Li, G., Liu, X., Tang, J., Li, J., Ren, Z., & Chen, C. (2020). De-noising low-frequency magnetotelluric data using mathematical morphology filtering and sparse representation. Journal of Applied Geophysics, 172, 103919. doi:10.1016/j.jappgeo.2019.103919.

[18] Wang, P., Chen, X., & Zhang, Y. (2023). Synthesizing magnetotelluric time series based on forward modeling. Frontiers in Earth Science, 11(February), 1–13. doi:10.3389/feart.2023.1086749.

[19] Yang, Y., Zhang, H., Zhu, Y., Zhou, C., & Sun, H. (2023). Denoising land-based controlled-source electromagnetic data based on a same-site noise reference channel. Geophysical Journal International, 235(3), 2285–2304. doi:10.1093/gji/ggad361.

[20] Bergen, K. J., Johnson, P. A., de Hoop, M. V., & Beroza, G. C. (2019). Machine learning for data-driven discovery in solid Earth geoscience. Science, 363(6433), eaau0323. doi:10.1126/science.aau0323.

[21] Dramsch, J. S. (2020). 70 Years of Machine Learning in Geoscience in Review. Advances in Geophysics, 61(January), 1–55. doi:10.1016/bs.agph.2020.08.002.

[22] Rau, E. G. (2022). Application of Machine Learning and Magnetotellurics to Aid in Subsurface Characterization of Petroleum and Geothermal Reservoirs. Doctoral dissertation, Baylor University, Texas, United States.

[23] Marzan, I., Martí, D., Lobo, A., Alcalde, J., Ruiz, M., Alvarez-Marron, J., & Carbonell, R. (2021). Joint interpretation of geophysical data: Applying machine learning to the modeling of an evaporitic sequence in Villar de Cañas (Spain). Engineering Geology, 288(August 2020), 106126. doi:10.1016/j.enggeo.2021.106126.

[24] Utama, W., Indriani, R. F., Hermana, M., Anjasmara, I. M., Garini, S. A., & Putra, D. P. N. (2024). Towards Improving Sustainable Water Management in Geothermal Fields: SVM and RF Land Use Monitoring. Journal of Human, Earth, and Future, 5(2), 216–242. doi:10.28991/HEF-2024-05-02-06.

[25] Abbasi, F. A., Sajjad, A., Ayubi, M., Haider, G., Lalji, S. M., Ali, S. I., & Burney, M. (2024). Predicting permeability in sandstone reservoirs from mercury injection capillary pressure data using advanced machine learning algorithms. Arabian Journal of Geosciences, 17(12), 1–18. doi:10.1007/s12517-024-12145-6.

[26] Li, J., Liu, Y., Tang, J., & Ma, F. (2023). Magnetotelluric noise suppression via convolutional neural network. Geophysics, 88(1), WA361–WA375. doi:10.1190/geo2022-0258.1.

[27] Pichika, S. V. V. S. N., Chaitanya, M. Y., Rajasekharan, S. G., & Yadav, R. (2023). Comparison of noise reduction performance of denoising autoencoders with CNN and LSTM. AIP Conference Proceedings, 2715, 1–5. doi:10.1063/5.0134232.

[28] Legowo, N., & Bad, W. M. (2024). Outlier Detection in VPN Authentication Logs for Corporate Computer Networks Access using CRISP-DM. HighTech and Innovation Journal, 5(4), 1101-1117. doi:10.28991/HIJ-2024-05-04-016.

[29] Chen, J., Du, L., Guo, G., Yin, L., & Wei, D. (2022). Target-attentional CNN for Radar Automatic Target Recognition with HRRP. Signal Processing, 196, 108497. doi:10.1016/j.sigpro.2022.108497.

[30] Yu, N., Ji, M., Zhang, C., Ye, Y., & Zhou, W. (2025). A novel frequency-division deep-learning approach for magnetotelluric data quality enhancement. Geophysics, 90(3), WA169–WA187. doi:10.1190/geo2024-0451.1.

[31] Li, G., Gu, X., Chen, C., Zhou, C., Xiao, D., Wan, W., & Cai, H. (2024). Low-Frequency Magnetotelluric Data Denoising Using Improved Denoising Convolutional Neural Network and Gated Recurrent Unit. IEEE Transactions on Geoscience and Remote Sensing, 62, 1–16. doi:10.1109/TGRS.2024.3374950.

[32] Liu, Z., Chen, H., Ren, Z., Tang, J., Xu, Z., Chen, Y., & Liu, X. (2021). Deep learning audio magnetotellurics inversion using residual-based deep convolution neural network. Journal of Applied Geophysics, 188, 104309. doi:10.1016/j.jappgeo.2021.104309.

[33] Pal, U., Chattopadhyay, P. B., Sarraf, Y., & Halder, S. (2025). Optimizing noise reduction in layered-earth magnetotelluric data for generating smooth models with artificial neural networks. Acta Geophysica, 73(2), 1449–1479. doi:10.1007/s11600-024-01434-z.

[34] Li, J., Cheng, H., Wang, J., Zhang, X., & Tang, J. (2024). Coordinate Attention-Temporal Convolutional Network for Magnetotelluric Data Processing. IEEE Transactions on Geoscience and Remote Sensing, 62, 1–14. doi:10.1109/TGRS.2024.3418042.

[35] Wan, S. (2024). A Denoising Time Window Algorithm for Optimizing LSTM Prediction. IEEE Access, 12(March), 74268–74290. doi:10.1109/ACCESS.2024.3404456.

[36] Gui, T., Deng, J., Li, G., Chen, H., Yu, H., & Feng, M. (2024). De-noising magnetotelluric data based on machine learning. Journal of Applied Geophysics, 230(March), 105538. doi:10.1016/j.jappgeo.2024.105538.

[37] Ji, M., Chen, H., Zhang, C., Yu, N., & Kong, W. (2024). A Magnetotelluric Data Denoising Method Based on Lightweight Ensemble Learning. IEEE Transactions on Geoscience and Remote Sensing, 62, 1–13. doi:10.1109/TGRS.2024.3401194.

[38] Vozar, J., Jones, A. G., Campanya, J., Yeomans, C., Muller, M. R., & Pasquali, R. (2020). A geothermal aquifer in the dilation zones on the southern margin of the Dublin Basin. Geophysical Journal International, 220(3), 1717–1734. doi:10.1093/gji/ggz530.

[39] Aizawa, K., Koyama, T., Hase, H., Uyeshima, M., Kanda, W., Utsugi, M., Yoshimura, R., Yamaya, Y., Hashimoto, T., Yamazaki, K., Komatsu, S., Watanabe, A., Miyakawa, K., & Ogawa, Y. (2014). Three-dimensional resistivity structure and magma plumbing system of the Kirishima Volcanoes as inferred from broadband magnetotelluric data. Journal of Geophysical Research: Solid Earth, 119(1), 198–215. doi:10.1002/2013JB010682.

[40] Puppala, H., Saikia, P., Kocherlakota, P., & Suriapparao, D. V. (2023). Evaluating the applicability of neural network to determine the extractable temperature from a shallow reservoir of Puga geothermal field. International Journal of Thermofluids, 17(November 2022), 100259. doi:10.1016/j.ijft.2022.100259.

[41] Li, Y., Li, T., Chen, H., & Li, X. (2022). Design of intelligent monitoring and management software for Taiwan-level drop-out fuse. 2022 IEEE 10th Joint International Information Technology and Artificial Intelligence Conference (ITAIC), 10, 1528-1531. doi:10.1109/ITAIC54216.2022.9836496.

[42] Ebtehaj, I., & Bonakdari, H. (2024). CNN vs. LSTM: A Comparative Study of Hourly Precipitation Intensity Prediction as a Key Factor in Flood Forecasting Frameworks. Atmosphere, 15(9), 1082. doi:10.3390/atmos15091082.

[43] Zhen, L., & Bărbulescu, A. (2024). Comparative Analysis of Convolutional Neural Network-Long Short-Term Memory, Sparrow Search Algorithm-Backpropagation Neural Network, and Particle Swarm Optimization-Extreme Learning Machine Models for the Water Discharge of the Buzău River, Romania. Water (Switzerland), 16(2), 289. doi:10.3390/w16020289.

[44] Zuo, G., Ren, Z., Xiao, X., Tang, J., Zhang, L., & Li, G. (2022). Magnetotelluric Noise Attenuation Using a Deep Residual Shrinkage Network. Minerals, 12(9), 1086. doi:10.3390/min12091086.

[45] Singh, D., & Singh, B. (2020). Investigating the impact of data normalization on classification performance. Applied Soft Computing, 97, 105524. doi:10.1016/j.asoc.2019.105524.

[46] Li, J., Liu, Y., Tang, J., Peng, Y., Zhang, X., & Li, Y. (2023). Magnetotelluric data denoising method combining two deep-learning-based models. Geophysics, 88(1), E13–E28. doi:10.1190/geo2021-0449.1.

[47] Pavlatos, C., Makris, E., Fotis, G., Vita, V., & Mladenov, V. (2023). Enhancing Electrical Load Prediction Using a Bidirectional LSTM Neural Network. Electronics (Switzerland), 12(22), 1–13. doi:10.3390/electronics12224652.

[48] Priyanka, Kumari, A., & Sood, M. (2021). Implementation of SimpleRNN and LSTMs based prediction model for coronavirus disease (Covid-19). IOP Conference Series: Materials Science and Engineering, 1022(1), 012015. doi:10.1088/1757-899X/1022/1/012015.

[49] Van Houdt, G., Mosquera, C., & Nápoles, G. (2020). A review on the long short-term memory model. Artificial Intelligence Review, 53(8), 5929–5955. doi:10.1007/s10462-020-09838-1.

[50] Ghimire, S., Deo, R. C., Wang, H., Al-Musaylh, M. S., Casillas-Pérez, D., & Salcedo-Sanz, S. (2022). Stacked LSTM Sequence-to-Sequence Autoencoder with Feature Selection for Daily Solar Radiation Prediction: A Review and New Modeling Results. Energies, 15(3), 1–39. doi:10.3390/en15031061.

[51] Liao, X., Zhang, Z., Yan, Q., Shi, Z., Xu, K., & Jia, D. (2022). Inversion of 1-D magnetotelluric data using CNN-LSTM hybrid network. Arabian Journal of Geosciences, 15(17), 1–9. doi:10.1007/s12517-022-10687-1.

[52] Wang, L., Yu, Z., Zhang, Y., & Yao, P. (2023). Review of machine learning methods applied to enhanced geothermal systems. Environmental Earth Sciences, 82(3), 1–19. doi:10.1007/s12665-023-10749-x.

[53] Amin, J., Sharif, M., Anjum, M. A., Raza, M., & Bukhari, S. A. C. (2020). Convolutional neural network with batch normalization for glioma and stroke lesion detection using MRI. Cognitive Systems Research, 59, 304–311. doi:10.1016/j.cogsys.2019.10.002.

[54] Imamverdiyev, Y., & Sukhostat, L. (2019). Lithological facies classification using deep convolutional neural network. Journal of Petroleum Science and Engineering, 174(October), 216–228. doi:10.1016/j.petrol.2018.11.023.

[55] Sarkalkan, N., Loeve, A. J., Van Dongen, K. W. A., Tuijthof, G. J. M., & Zadpoor, A. A. (2015). A novel ultrasound technique for detection of osteochondral defects in the ankle joint: A parametric and feasibility study. Sensors (Switzerland), 15(1), 148–165. doi:10.3390/s150100148.

[56] Lee, C. C., Koo, V. C., Lim, T. S., Lee, Y. P., & Abidin, H. (2022). A multi-layer perceptron-based approach for early detection of BSR disease in oil palm trees using hyperspectral images. Heliyon, 8(4), e09252. doi:10.1016/j.heliyon.2022.e09252.

[57] Xu, B., An, Z., Han, Y., & Ye, G. (2024). Denoising CSAMT signals in the time domain based on long short-term memory. Journal of Geophysics and Engineering, 21(2), 507–516. doi:10.1093/jge/gxae017.

[58] Jin, J., Zhang, Y., Hao, Z., Xia, R., Yang, W., Yin, H., & Zhang, X. (2022). Benchmarking data-driven rainfall-runoff modeling across 54 catchments in the Yellow River Basin: Overfitting, calibration length, dry frequency. Journal of Hydrology: Regional Studies, 42(April), 101119. doi:10.1016/j.ejrh.2022.101119.

[59] Ryu, K. H., Oh, S., & Kwon, H. S. (2024). Vehicle noise characteristics in magnetotelluric data and vehicle noise removal using waveform fitting. Journal of Applied Geophysics, 230(August), 105534. doi:10.1016/j.jappgeo.2024.105534.

[60] Wangwongchai, A., Waqas, M., Dechpichai, P., Hlaing, P. T., Ahmad, S., & Humphries, U. W. (2023). Imputation of missing daily rainfall data; A comparison between artificial intelligence and statistical techniques. MethodsX, 11(September), 102459. doi:10.1016/j.mex.2023.102459.

[61] Ogawa, H., Asamori, K., Negi, T., & Ueda, T. (2023). A novel method for processing noisy magnetotelluric data based on independence of signal sources and continuity of response functions. Journal of Applied Geophysics, 213(September), 105012. doi:10.1016/j.jappgeo.2023.105012.

[62] Garini, S. A., Shiddiqi, A. M., Utama, W., Jabar, O. A., & Insani, A. N. F. (2024). Enhanced Lithology Classification in Well Log Data Using Ensemble Machine Learning Techniques. 2024 IEEE International Conference on Artificial Intelligence and Mechatronics Systems (AIMS), 1-8. doi:10.1109/AIMS61812.2024.10512485.